NATIONAL AERONAUTICS AND SPACE ADMINISTRATION
LANGLEY RESEARCH CENTER
LANGLEY STATION
HAMPTON, VIRGINIA 23365

IN REPLY REFER TO:

Agency Code 126-14-03-18

DEC 10 1965

N66-16486

TO: NASA Headquarters - Code RTR
           Attention: T. T. Neill

FROM: Director

SUBJECT: Transmittal of prospective Contractor Report CR-66039
             entitled "Development of a Photoelasto-Plastic Method
             to Study Stress Distributions in Vicinity of a Simulated
             Crack - Phases I and II" by A. R. Hunter of Lockheed
             Missiles and Space Company, Sunnyvale, California

The subject report is recommended for Contractor Report 50,000 series, outside distribution upon request.

Contract NAS1-4760 funded by Office of Advanced Research and Technology.

Langley technical monitor - Herbert F. Hardrath

It is requested that Langley be notified when the subject report is approved.

Floyd L. Thompson

Enclosure

cc: NASA Code RA w/enc.

Concur in Langley's recommendation that subject report be published as high number CR.

H L Brown 1/10/66

TITLE: Development of a Photoelasto-plastic Method to Study Stress
         Distributions in Vicinity of a Simulated Crack - Phases I and II

BY: A. R. Hunter, Lockheed Missiles and Space Company

ABSTRACT

A new photoelasto-plastic technique is presented. This method utilizes
the creep characteristics of polymer materials at elevated temperatures
to simulate stress-strain behavior of aluminum alloys. Through the use
of frozen stress and slicing procedures, the technique has been applied
for three-dimensional stress analyses.

An evaluation of the method has been made through the study of flat
specimens containing a central hole. Several ratios of thickness to
hole diameters and several levels of local plasticity were investigated.
A close correlation was found between the experimental results and theoretical
analyses.

JHCrews:cam   11-23-65

HFH 11-23-65

RRH 11-24-65

DEVELOPMENT OF
A PHOTOELASTO-PLASTIC METHOD
TO STUDY STRESS DISTRIBUTIONS
IN VICINITY OF A SIMULATED
CRACK – PHASE I AND II

by

A. R. Hunter

4-05-65-11   October 1965

FOREWORD

This report has been prepared by Lockheed Missiles and Space Company for the Langley Research Center of the National Aeronautics and Space Administration under contract No. NAS 1-4760. This report describes the development of a photoelasto-plastic method to study the elasto-plastic stress distributions in plates containing notches utilizing "frozen stress" techniques. The results can be applied to aluminum alloys.

SUMMARY

The purpose of this program was to develop a photoelasto-plastic stress analysis method which could be used to study experimentally the stress distributions in the vicinity of simulated cracks. This method utilizes the frozen stress and creep characteristics of plastic materials to simulate the stress-strain behavior of aluminum alloys. Two polymer materials were subjected to various thermal cycles, the maximum temperatures of which were significantly below the critical temperature. Below the critical temperature, polymer materials normally used in photoelasticity experience considerable creep. The strain and birefringence associated with this creep can be frozen into certain materials and subsequently sliced without relieving the frozen strain.

A material and thermal cycle was selected which exhibited an effective stress-strain curve similar to the uniaxial stress-strain behavior of 2024-T3 aluminum alloy. "Infinite plate" models were machined from the selected material and subjected to constant tensile load and the appropriate thermal cycle to simulate 2024-T3 aluminum. The infinite plate models contained centrally located holes 1/8 in. in diameter.

Two thin plate models (1/8-in. thick) were subjected to tensile loads corresponding to $\sigma_\infty/\sigma_1 = 0.11$ and 0.71. The stress distribution along a centerline normal to the direction of loading was determined for the two cases of $\sigma_\infty/\sigma_1 = 0.11$ and 0.71.

Two thick plate models (0.4-in. thick) were subjected to tensile loads corresponding to $\sigma_\infty/\sigma_1 = 0.41$, 0.53. The stress distributions were determined adjacent to the hole along a line normal to the direction of load at the surface and the midplane.

LOCKHEED MISSILES & SPACE COMPANY

The stress concentration factors determined for the infinite plates are in very good agreement with theory. The stress concentration factors for the thick plates were slightly higher at the midplane of the plates than at the surface. Due to the higher stresses at the midplane of the thick plates, there results a σ_z stress normal to the load direction and parallel to hole direction. This σ_z stress is maximum at the midplane and edge of hole and diminishes to zero a short distance from the hole.

It is clearly illustrated that the photoelasto-plastic method can be used to determine elasto-plastic stress concentration factors for aluminum alloys. Also realistic results are obtained for stress variation through the thickness of notched plates. Therefore, it is recommended that this method be applied to the study of plates containing simulated cracks. Information concerning the three-dimensional flow in the vicinity of cracks in aluminum alloys cannot be obtained by any other presently available experimental technique.

CONTENTS

ILLUSTRATIONS

LOCKHEED MISSILES & SPACE COMPANY

Section 1

INTRODUCTION

1.1 SCOPE OF INVESTIGATION

The photoelasto-plastic method utilizes the creep and "frozen" stress characteristics exhibited by epoxy resins and other polymer materials when subjected to a thermal cycle whose maximum temperature is significantly less than the "critical" temperature of the material. The resulting "frozen" stress-strain behavior is characterized by the generation of nonlinear effective stress-strain curves. Effective stress-strain curves of this nature were generated for two materials, an epoxy and a polycarbonate for various thermal cycles in order to arrive at a material and associated thermal cycle which could be used to simulate the stress-strain behavior of an aluminum alloy. Also the associated birefringence was determined (calibration). Stress-strain simularity was established by use of the Ramberg-Osgood method of stress-strain representation. Upon selection of an appropriate model material and thermal cycle, elasto-plastic stress distributions were determined for infinite plates to verify the usefulness of the method. The ultimate goal of this program is the application of this photoelasto-plastic method of stress analysis to study stress distributions in the vicinity of a simulated crack.

1.2 BACKGROUND

Neuber (Ref. 1) has treated analytically the stress-distributions in the vicinity of a crack in an infinite plate. The analysis shows a very rapid decrease in stress level at the leading edge of the crack. Therefore, for small values of ℓ/w, the crack-length to plate-width ratio, an infinite plate behavior would be expected. For the case of intermediate values of ℓ/w, Brossman and Kies (Ref. 2) suggest that a correction factor be applied to the stress concentration factors as determined by Neuber's theory.

1

This correction factor is approximate and applies only for intermediate values of ℓ/w . According to Brossman and Kies, this correction factor is not necessary for values of ℓ/w less than 0.35. These methods are applicable only in the case of plane-stress.

The analytical solution of plane-stress plasticity problems of technical importance has proven to be forbiddingly complicated. Therefore, in recent years, attention has been given to experimental methods. The most popular experimental method is the use of bonded birefringent coatings. Wells and Post (Ref. 3) performed a photoelastic analysis of the dynamic stress distribution in the vicinity of a crack. Dixon (Ref. 4) has studied the effect of finite width for a centrally located crack. Dixon (Ref. 5) and Kawata (Ref. 6) have studied the elasto-plastic strain distributions for notches using the bonded bire-fringent coating method. Gerberich (Ref. 7) has applied the coating method to study strain distribution about a slowly growing crack. These methods assume elastic stress distributions and plane stress or only surface strains in the plastic range. It is known that even in the elastic range, the stress distribution is not uniform through the plate thickness for thick plates subjected to simple tension. This situation is more signifi-cant in the plastic range. Therefore, a three-dimensional method is needed. The developed photoelasto-plastic method described in this report could fulfill this need. In addition, this method could be utilized to study a wide variety of plasticity problems, particularly in design problems where it is desirable to utilize structural material in the plastic range to achieve high-strength and minimum-weight characteristics.

Section 2

TECHNICAL APPROACH

2.1 PHOTOELASTO-PLASTIC THEORY

The behavior of some photoelastic materials is elastic above a "critical" temperature. Therefore, using the "frozen stress" technique, it is possible to study three-dimensional elastic stress distribution in structural models by examination of slices removed from the models. This technique is well established and has provided very useful information concerning stress concentrations and stress distributions associated with very complex engineering structures.

At room temperature and temperature well below the critical temperature, some photoelastic materials experience a significant amount of creep. The occurrence of creep results in an effective stress-strain curve which is nonlinear. This behavior can be utilized in such a way as to provide a means of studying elasto-plastic stress distributions. The "frozen" stress feature provides for extension to three-dimensional situations.

The "frozen stress" method consists of application of a load to a transparent plastic model at room temperature. The model is then brought to the critical temperature of the model material and then slowly cooled (to prevent thermal stresses) to room temperature. Upon removal of the load a stress pattern similar to that which would have existed at room temperature may be observed. In addition, the model may be sliced without relieving the "frozen stress" fringe pattern. This photoelastic fringe pattern represents an elastic stress distribution. An understanding of this phenomena can be obtained by consideration of the "Multiphase Theory of Plastics" by Kuske*

---

*A. Kuske, "Multiphase Theory of Plastics," Experimental Mechanics, Sept. 1962, p. 278

3

Plastics may be considered to consist of two phases: an elastic phase and a plastic phase. Birefringence results from a contribution by each phase and can be expressed as

$$\Delta = C_p t(\sigma_1 - \sigma_2)_p + C_e t(\sigma_1 - \sigma_2)_e \tag{1}$$

where

$$
\begin{aligned}
c &= \text{stress optical coefficient} \\
t &= \text{optical path} \\
\sigma_1 - \sigma_2 &= \text{principal stress difference} \\
p &= \text{pertaining to plastic phase} \\
e &= \text{pertaining to elastic phase}
\end{aligned}
$$

The stress optical coefficients C_p and C_e are constants which depend upon the material. They are independent of temperature. The modulus of the elastic phase (E_e) is also independent of temperature. The modulus of the plastic phase (E_p) is a function of temperature, time and stress. When the photoelastic model is stressed, a portion of the stress is carried by each phase depending upon the relative modulus values of the two phases. At room temperature $E_p \gg E_e$ and the stress in the elastic phase is insignificant. As the temperature is increased, the modulus E_p decreases and we find that the elastic phase carries more and more of the load until at the "critical" temperature $(E_p = 0)$ all the load is carried by the elastic phase. Then Eq. (1) becomes

$$\Delta = C_e t(\sigma_1 - \sigma_2)_e \tag{2}$$

Therefore, the material behaves elastically at the "critical" temperature. Upon slowly cooling to room temperature, the plastic phase hardens, thus "freezing" the elastic phase in a state of deformation. Upon removal of the load, the photoelastic pattern remains. Slicing does not disturb this pattern since it is "frozen" on a molecular scale. Thus, slices may be removed from the model and stresses determined in the plane of the slices.

4

If a loaded photoelastic model is subjected to a thermal cycle of T_{max} significantly less than the critical temperature for the material, appreciable creep will be observed. In terms of the multi-phase theory, the modulus of the plastic phase diminishes with time and more load is carried by the elastic phase, resulting in a higher stress in this phase and greater elongation. Utilizing this creep feature, it is possible to generate an "effective" stress-strain curve that has nonlinear characteristics. "Effective" stress-strain curve refers to the relation between the "frozen stress" and strain defined as the permanent deformation per unit length measured after the specimen has undergone a specific thermal cycle.

It a simple tensile specimen experiences a given stress level (σ_1) at room temperature and then is subjected to a specific thermal cycle (Fig. 1) while under load, the resulting strain is composed of the elastic strain at maximum temperature and the strain resulting from creep which takes place during the thermal cycle. For various stress levels ($\sigma_1 > \sigma_2 > \sigma_3 > \ldots$), the resulting strains ($\epsilon_1 > \epsilon_2 > \epsilon_3 > \ldots$) are frozen into the material. From these data an effective stress-strain curve can be constructed which would represent the "frozen" stress-strain characteristics of the material for a given thermal cycle. Figure 2 represents a type of curve constructed in this manner. As a result of the "frozen" strain, there corresponds a birefringence which is also frozen into the material due to the loading and thermal cycle. Measurement of this birefringence yields a curve of the type shown in Fig. 3. This amounts to essentially the calibration.

After establishing the frozen stress-strain-birefringence characteristics for a given material and thermal cycle, a structural model may be subjected to a load system and the thermal cycle used in the calibration. Analysis of "frozen" birefringence in the structural model may then be interpreted in terms of the stress using the effective stress-birefringence curve. The experimental results obtained in this manner can be applied to any material that exhibited a stress-strain curve similar to the "effective" stress-strain obtained for the model material.
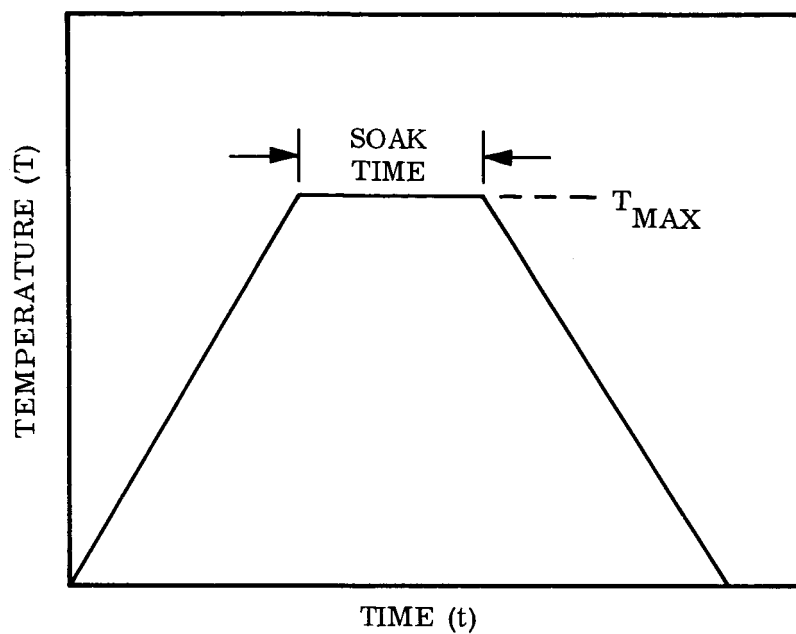
LOCKHEED MISSILES & SPACE COMPANY
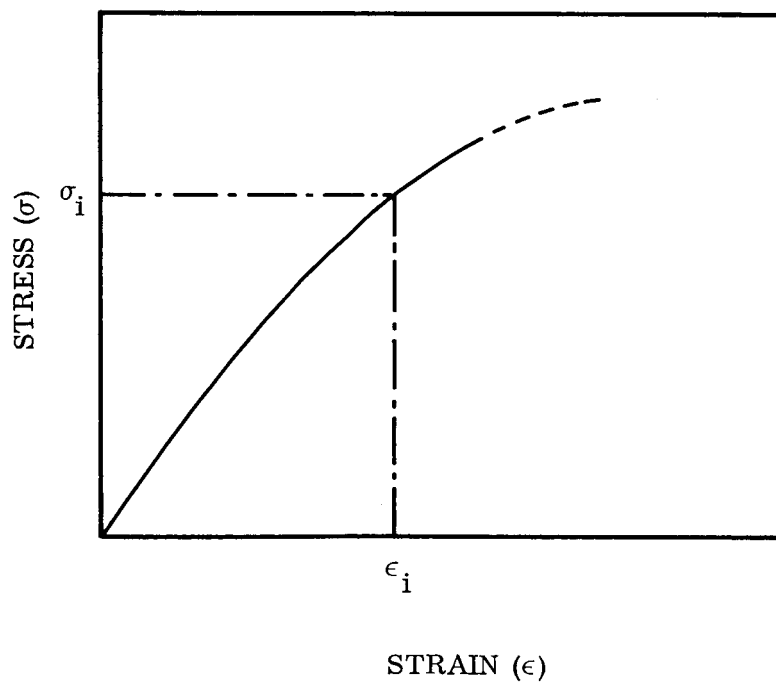
Fig. 1 Typical Thermal Cycle
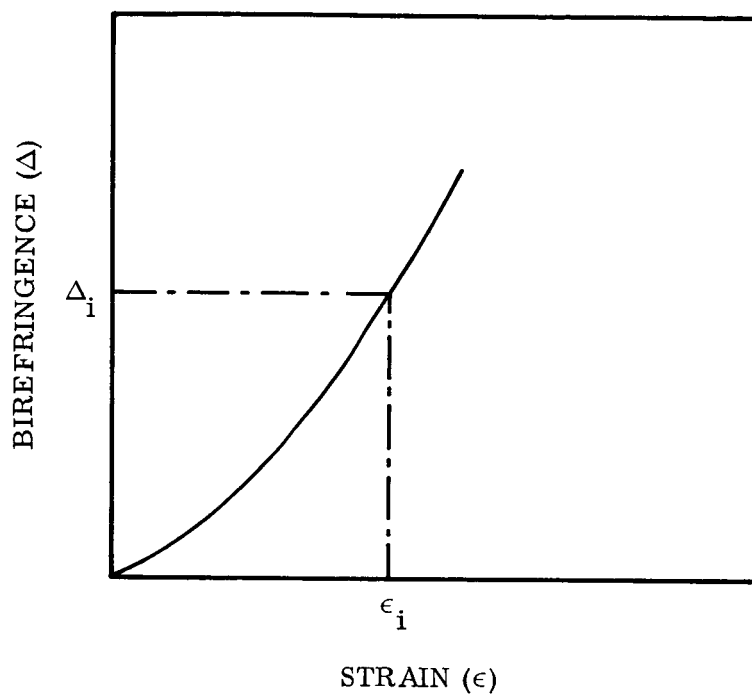

Fig. 2 Typical Effective Stress-Strain Curve

6

Fig. 3 Typical Birefringence Strain Curve

2.2 STRESS-STRAIN SIMILARITY

Ramberg and Osgood (Ref. 9) have suggested a relation to describe stress-strain curves for materials. This relationship is

$$e = \frac{S}{E} + K\left(\frac{S}{E}\right)^n \tag{3}$$

where

$$
\begin{aligned}
e &= \text{strain} \\
S &= \text{stress} \\
E &= \text{modulus of elasticity} \\
K \text{ and } n &= \text{material constants}
\end{aligned}
$$

This equation in dimensionless form is

$$\epsilon = \sigma + \frac{1 - m_1}{m_1} \sigma^n \tag{4}$$

where

$$\epsilon = \frac{eE}{S_1}$$

$$\sigma = \frac{S}{S_1}$$

$$S_1 = \text{secant yield strength } (E_1 = m_1 E)$$

Also, m_1 represents a chosen constant $0 < m_1 < 1$. Choosing $m_1 = 0.7$, Eq. (4) becomes

$$\epsilon = \sigma + \frac{3}{7} \sigma^n \tag{5}$$

Equation (5) represents all stress-strain curves which have the same shape factor n. Therefore, the "effective" stress-strain curve of the model material must have the same shape factor as the stress-strain curve for the prototype material in order that similarity exist.

8

Section 3

EXPERIMENTAL PROGRAM

3.1 CALIBRATION PHASE

3.1.1 Test Procedure

During the calibration phase of this program two materials were investigated, an epoxy resin cured with 10 pbw* of diethanolamine curing agent and a polycarbonate material.

The epoxy material was purchased in liquid resin form and cured in sheets 30 in. × 15 in. × 1/2 in. From these sheets 0.1-in. thick tensile specimens were machined. Even though the calibration specimens were only 0.1-in. thick, it was necessary to prepare them from thick plates so that the calibration would be applicable to the thick infinite plates, since the properties of polymers are to some degree a function of the casting mass. Figure 4 shows an as-cast plate of the epoxy material along with the mold.

The polycarbonate material was purchased in precast sheet 1/8-in. thick from which the calibration specimens were machined. The polycarbonate material, as received, possesses considerable residual stresses in the plane of the sheet and a large stress distribution through the thickness. Therefore, it was necessary to stress relieve the polycarbonate material before testing. Stress relief was accomplished by heating slowly (5° F/hr) to 325° F and soaking at this temperature for approximately 12 hours and then cooling slowly (5° F/hr) to room temperature.

The specimen configuration is shown in Fig. 5. A 2-in. gage length was scribed on the specimen surface for gage-length measurement prior to and after the test. From these gage-length measurements the axial strain was determined. Gage-length measurements were performed utilizing the x-y micrometer stage mounted on the polariscope. This
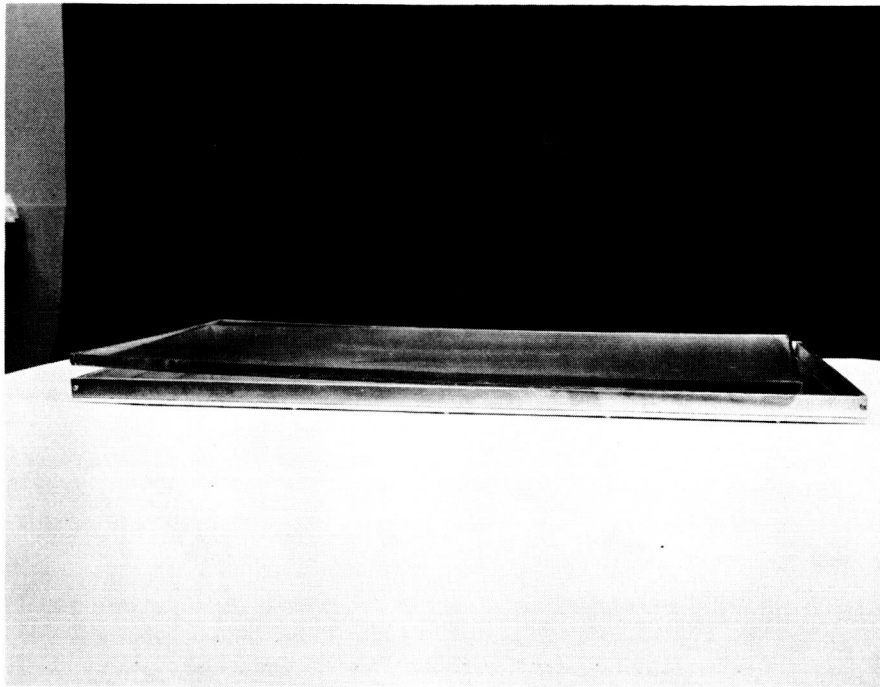
---

*parts by weight

9

Fig. 4 As-Cast Epoxy Plate and Associated Mold
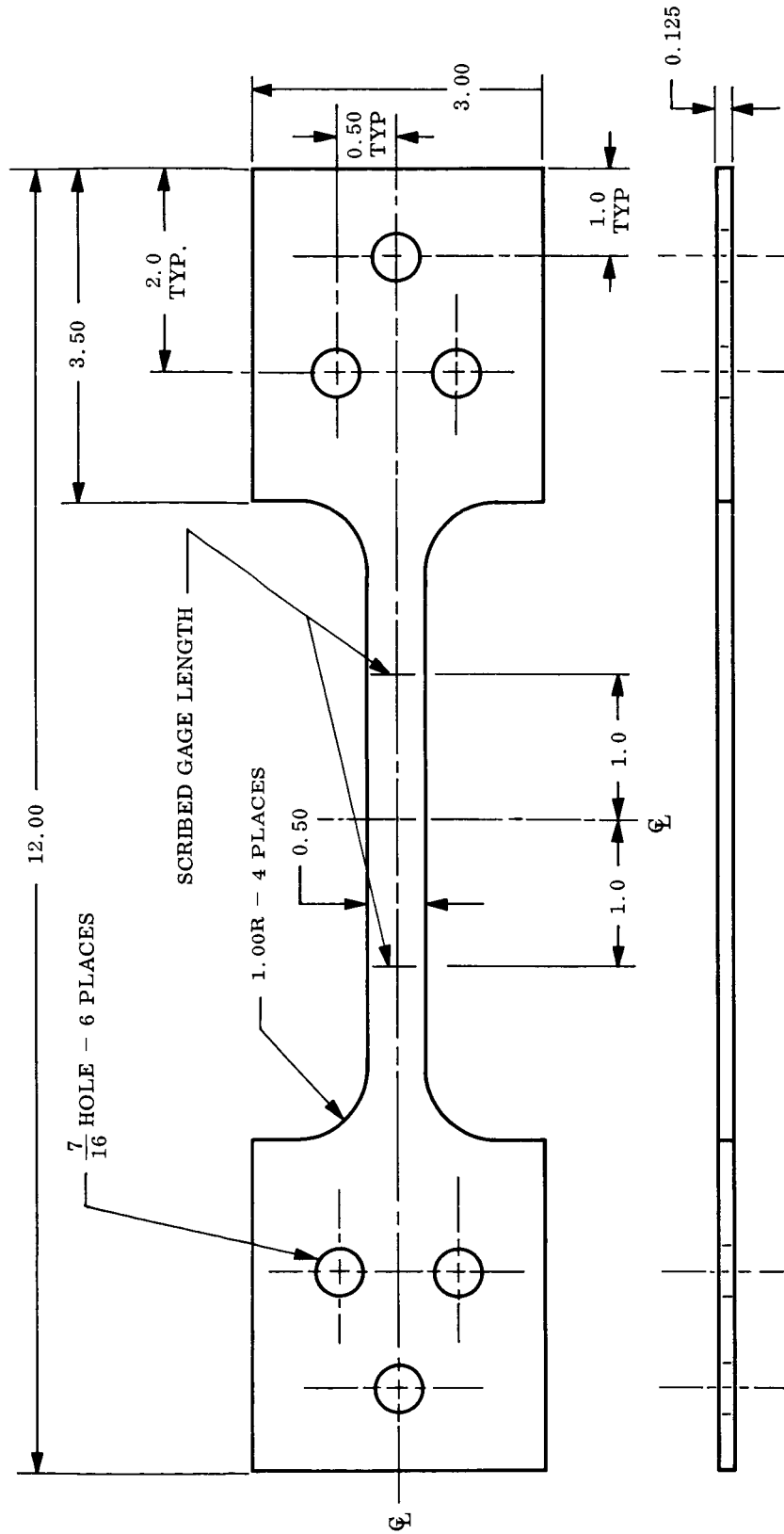
LOCKHEED MISSILES & SPACE COMPANY

Fig. 5 Calibration Specimen Configuration

11

micrometer stage has a 0.0001-in. readout. The specimen was mounted on the micrometer stage surface and the scribeline viewed on the ground-glass screen of the polariscope by use of transmitted light. The cross-hair marking on the ground-glass screen was placed at one of the scribe marks. The micrometer stage was adjusted until the other scribeline appeared at the cross-hair. The distance of the adjustment designates the gage length. The axial strain was computed from the change in gage length (before and after test) divided by the original gage length ($e = \Delta\ell/\ell_o$). Figure 6 shows the appearance of the scribe line on the ground-glass screen of the polariscope. The scribe line image is projected on the ground-glass screen as 10× magnification. After the initial gage lengths (ℓ_o) have been recorded along with the initial thickness (t_o) and width (w_o), the specimens are then subjected to dead-weight loads. The specimens and test frame are placed in the stress-freezing oven, as shown in Fig. 7. The specimens were then subjected to a programmed thermal cycle consisting of the appropriate maximum temperature (T_{max}), a heating-and-cooling rate of approximately 5° F/hr, and a soak time at T_{max} of two hours except where otherwise noted.

After completion of the thermal cycle, the specimens are unloaded and removed from the stress-freezing oven. Then the final gage lengths ℓ_f are measured in the manner previously described, along with t_f and w_f. Also, birefringence measurements are taken after testing. Figure 8 represents typical frozen fringe order distribution and indicates uniform stress in the reduced section of the calibration specimen.

3.1.2 Experimental Results (Calibration Phase)

From the experimental data, effective stress-strain curves, nondimensionalized stress-strain curves and birefringence-strain curves were constructed. These curves are represented in Figs. 9 through 19.

For the epoxy plus diethanolamine material, there are two sets of curves presented, designated as batch A and batch B. The only difference between batch A and batch B is that the material was cast at different times from a different lot of the basic epoxy

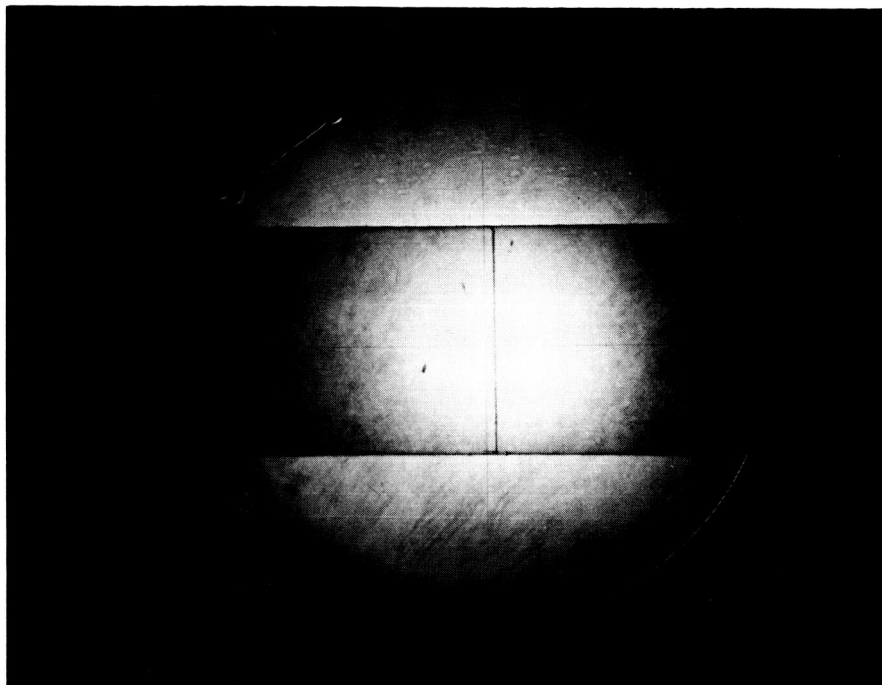**LOCKHEED MISSILES & SPACE COMPANY**

Fig. 6 Calibration Specimen Scribe Line as It Appears on Polariscope Projection Screen

Fig. 7 Loaded Calibration Specimens and Associated Test Frame in Furnace
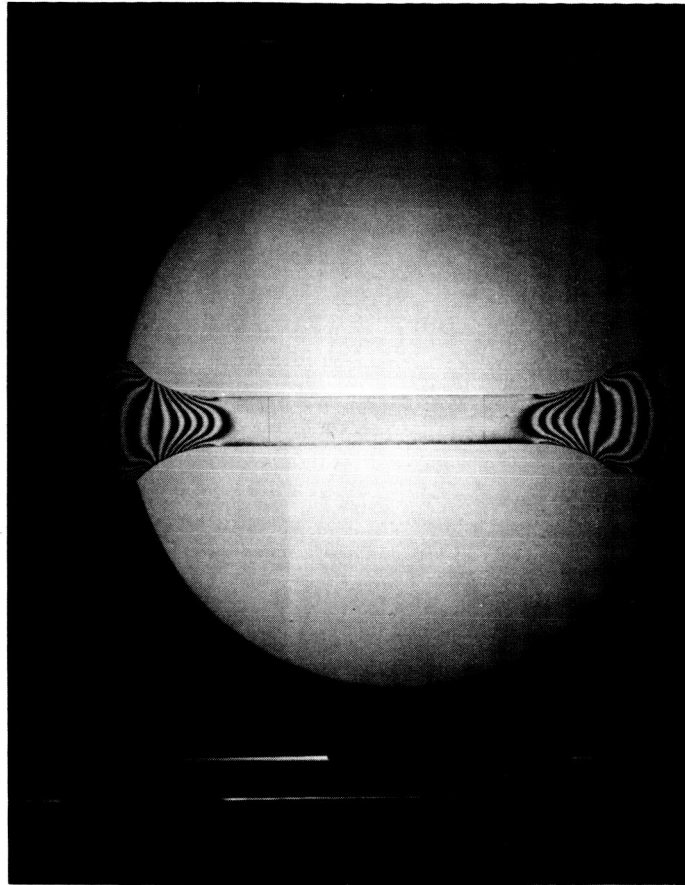
13

Fig. 8 Typical Frozen Stress Fringe Pattern for Calibration
Specimen

resin. It should be noted that the experimental data differ significantly between the two batches. Sufficient material (batch B) was cast from the same lot of basic resin (and at the same time) for calibration of the epoxy material and for analysis of infinite plates with holes.

Also, two sets of curves are presented for the polycarbonate material designated as batch A and batch B. The polycarbonate calibration specimens were prepared from 1/8-in. sheet stock, which is commercially available in already cast form. Sheets designated as batch A and batch B were purchased at different times and exhibited significantly different properties. This difference indicates that control of material properties is not part of the manufacturing procedure. It is even possible that manufacturing techniques were different for the two batches of material.

3.1.2.1 Epoxy Material (Batch B)

Effective stress-strain and birefringence curves were generated for the epoxy material (batch B) for thermal cycles consisting of maximum temperatures of 144, 150, 160, and 165°F. The heating-and-cooling rates of these thermal cycles were approximately 5°F/hr and soak time was two hours.

The effective stress-strain data for batch B are represented in Fig. 9. The nondimensionalized stress-strain curves are shown in Fig. 10 along with the nondimensionalized stress-strain data for 2024(24S-T) aluminum alloy. The nondimensionalized stress-strain curves for thermal cycles with T_{max} = 144, 150, and 160°F are identical and compare favorably with the aluminum alloy 2024(24S-T). Figure 11 represents the strain-birefringence curves for the thermal cycles of T_{max} = 144, 150, 160, and 165°F. The birefringence is approximately linearly related to strain.

3.1.2.2 Epoxy Material (Batch A)

Effective stress-strain and birefringence curves were generated for the epoxy material designated as batch A for four thermal cycles. Three of these thermal cycles
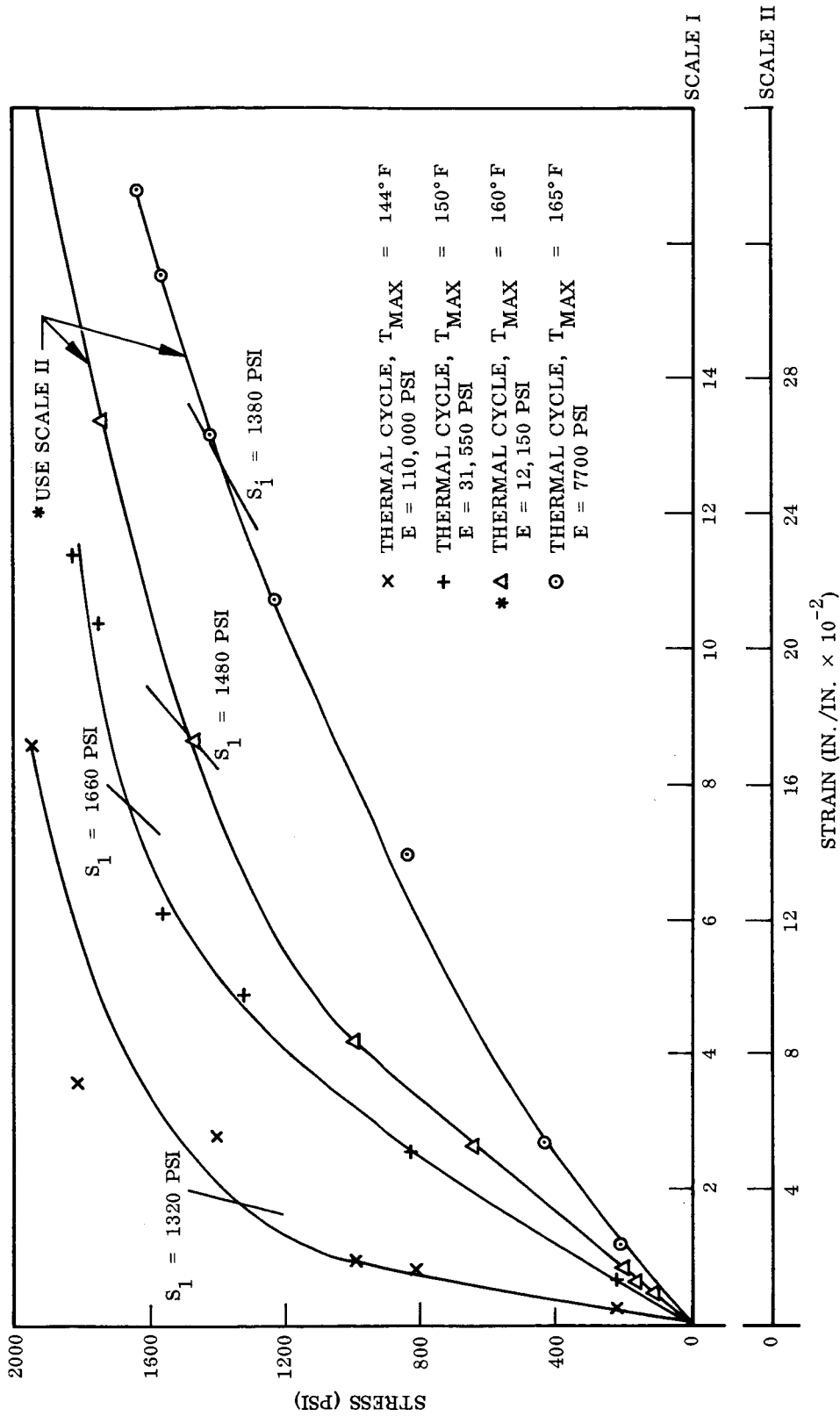
Fig. 9 Effective Stress-Strain Curves for Epoxy Material Batch B at Various Thermal Cycles
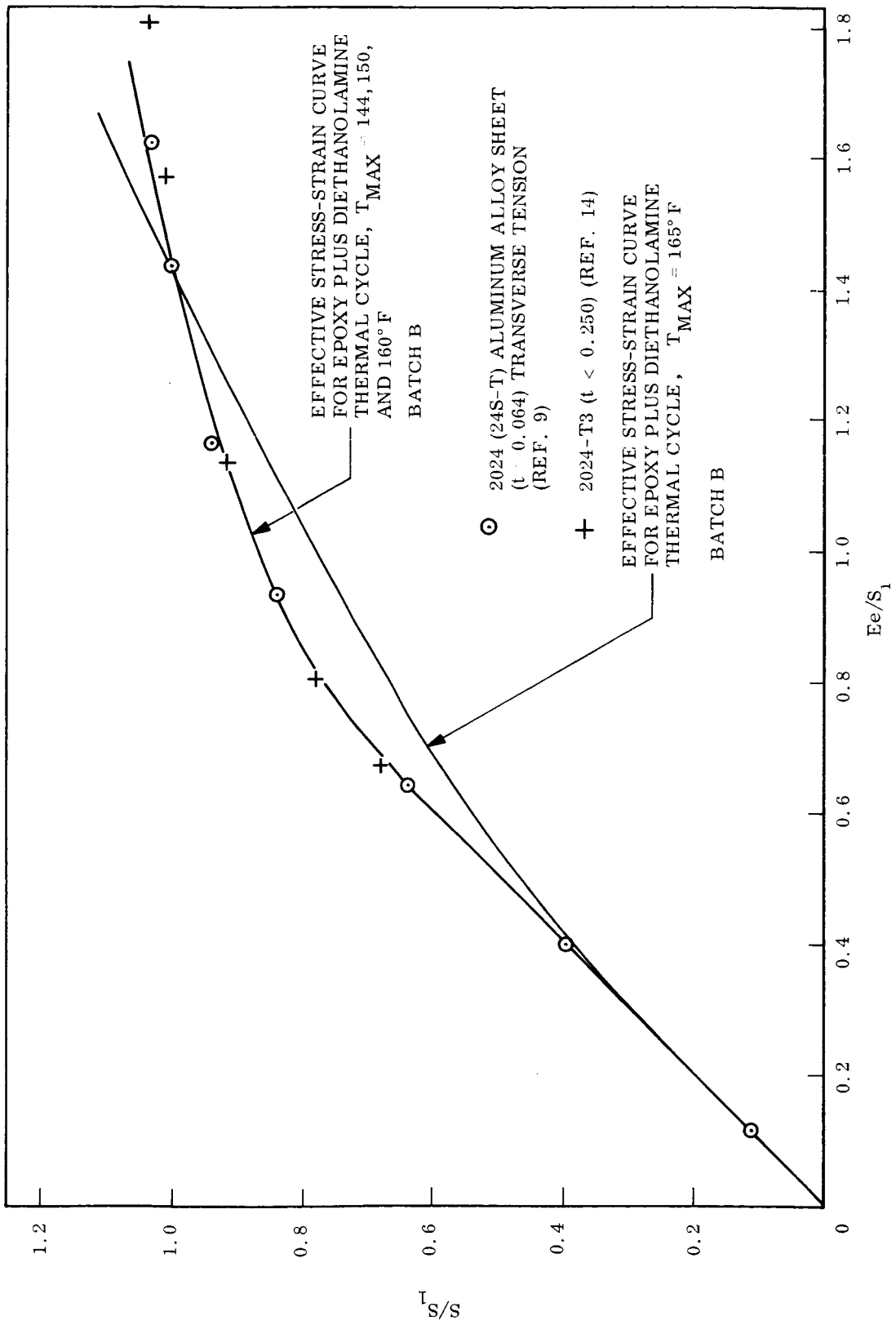
16

Fig. 10 Non-Dimensionalized Stress-Strain Curves for Epoxy Material Batch B

EFFECTIVE STRESS-STRAIN CURVE
FOR EPOXY PLUS DIETHANOLAMINE
THERMAL CYCLE, $T_{MAX} = 144, 150,$
AND 160° F

BATCH B

⊙   2024 (24S-T) ALUMINUM ALLOY SHEET
     (t 0.064) TRANSVERSE TENSION
     (REF. 9)

+   2024-T3 (t < 0.250) (REF. 14)

     EFFECTIVE STRESS-STRAIN CURVE
     FOR EPOXY PLUS DIETHANOLAMINE
     THERMAL CYCLE, $T_{MAX} = 165°$ F

     BATCH B

Ee/S_1

S/S_1

17

LOCKHEED MISSILES & SPACE COMPANY

Fig. 11 Strain–Birefringence Curves for Epoxy Material Batch B at Various Thermal Cycles

consisted of maximum temperatures of 165, 175, and 187° F, heating-and-cooling rates of 5° F per hour, and soak times of two hours. The remaining thermal cycle consisted of a maximum temperature of 175° F, heating rate of 440° F per hour, soak time of two hours, and a cooling rate of 5° F per hour. The effective stress-strain curves for batch A are represented in Fig. 12. It should be noted that the two thermal cycles with T_{max} = 175° F yield significantly different effective stress-strain curves. Since the creep characteristics of the materials are utilized in generating the effective stress-strain curves it would be expected that the effective stress-strain curve for high heating rates would be represented by strain values lower than those for low heating rates for comparable stress levels, due to the longer time duration for the test. The difference between the stress-strain curves for low and high rates indicates that some post curing (hardening) takes place during the heating portion of the cycle due to the longer time at temperature during the heating portion of the thermal cycle for the stress-strain curve with low heating rate. Even though there is a significant difference between the effective stress-strain curves for T_{max} = 175° F, these curves yield the same non-dimensionalized stress-strain curve which is similar to 2024(24S-T) aluminum alloy. The nondimensionalized stress-strain curves for epoxy material, batch A are shown in Fig. 13.

For batch A, a thermal cycle consisting of a maximum temperature of 187° F yields an elastic stress-strain curve and standard frozen-stress properties. In other words, the maximum temperature is near enough to the critical temperature of the material so that creep causes unloading of the plastic phase and complete loading of the elastic phase (loading of the molecular chain) during the thermal cycle.

Figure 14 represents the strain birefringence curves for batch A material. Strain is approximately linearly related to birefringence.
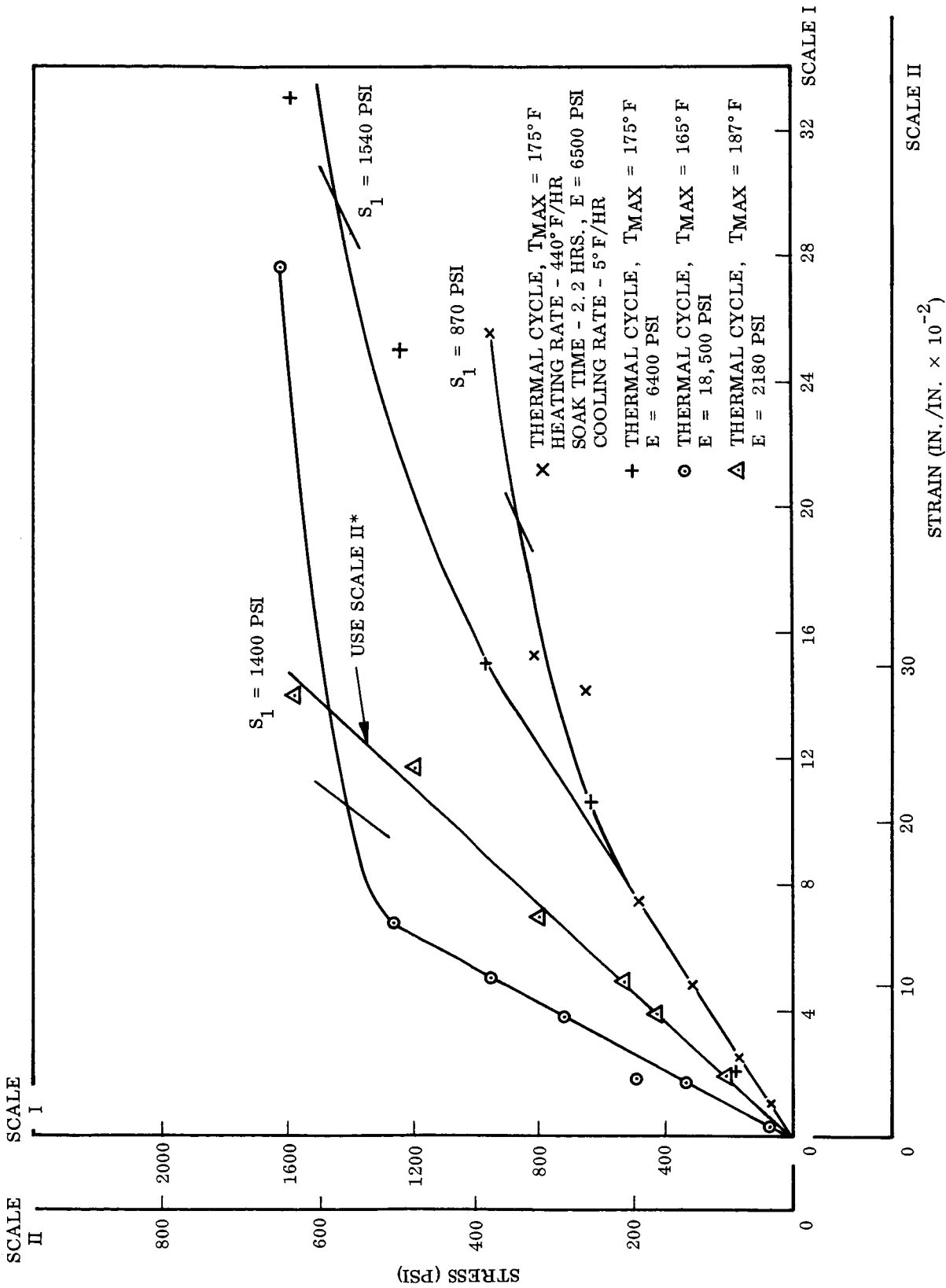
19

Fig. 12 Effective Stress-Strain Curves for Epoxy Material Batch A at Various Thermal Cycles.
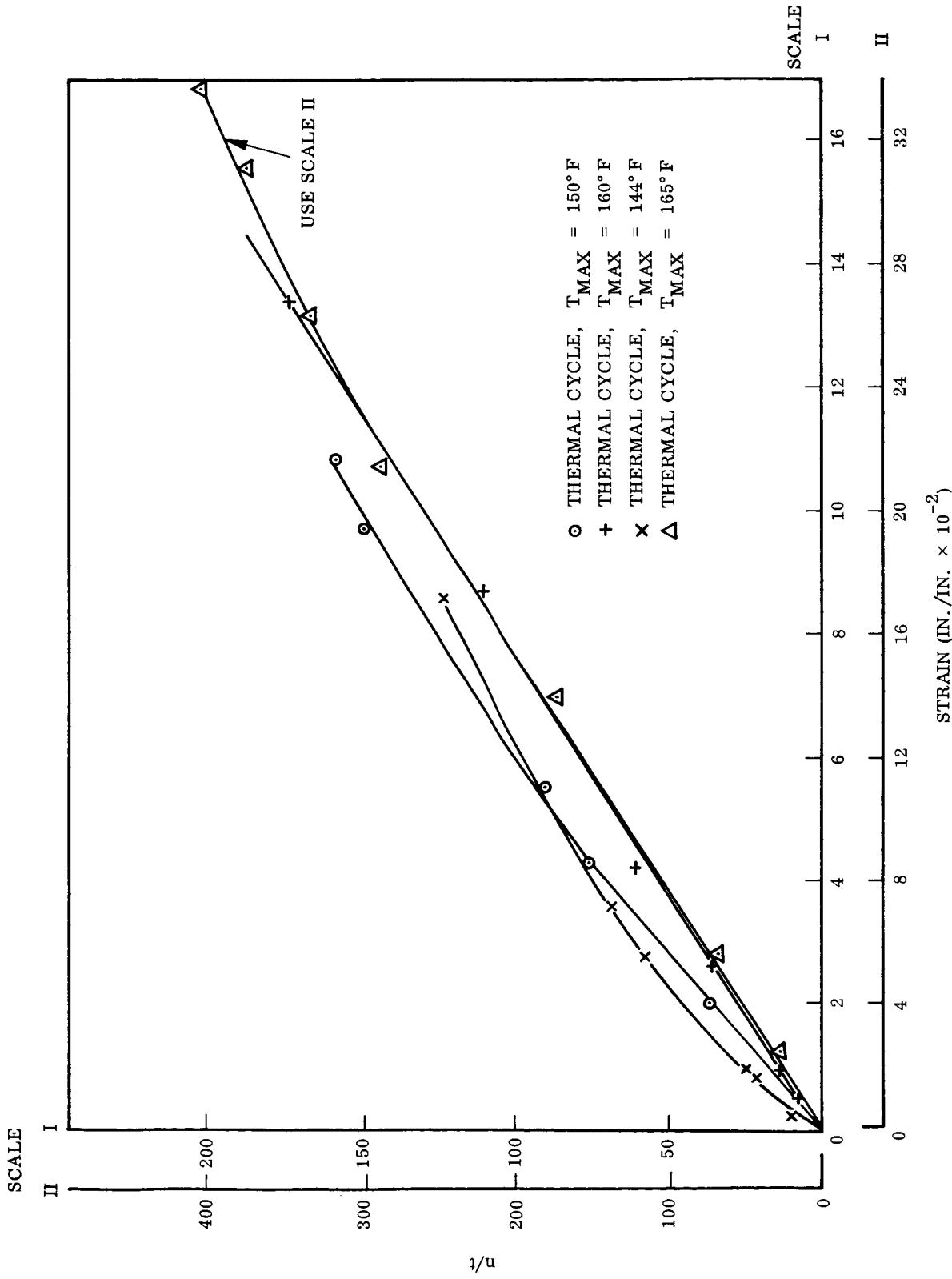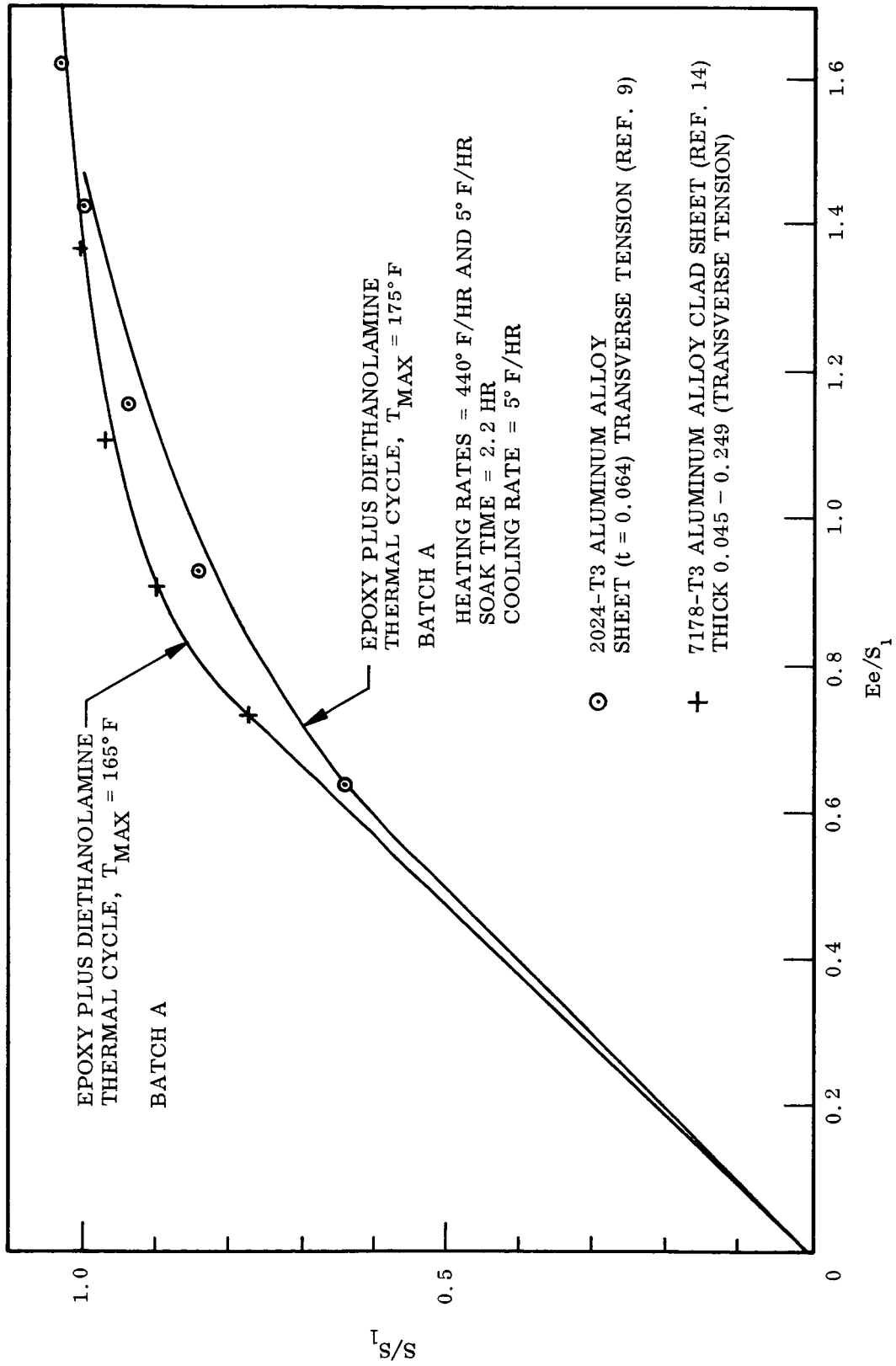
LOCKHEED MISSILES & SPACE COMPANY

Fig. 13 Non-Dimensionalized Stress-Strain Curves for Epoxy Material Batch A at Various Thermal Cycles
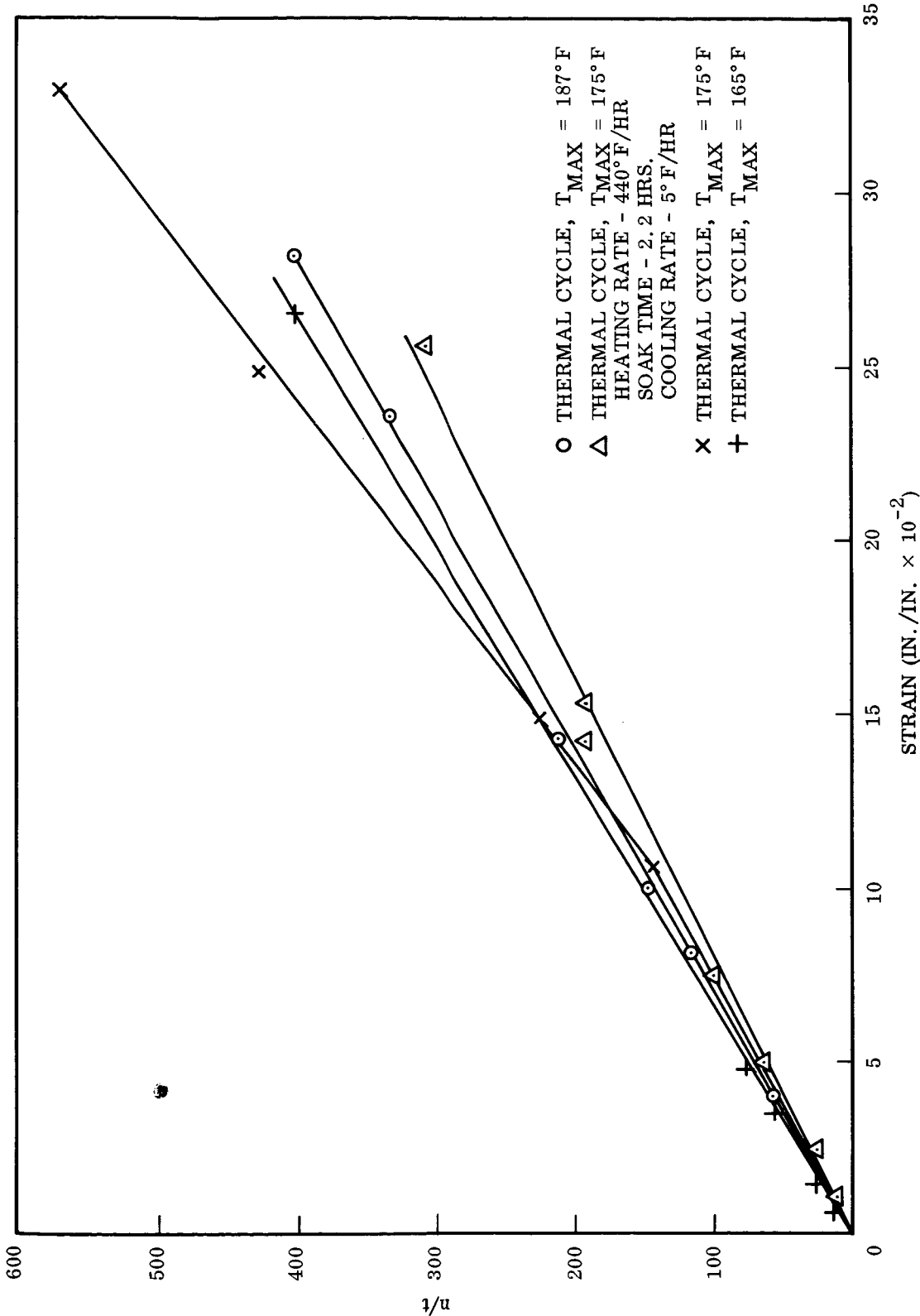
Fig. 14 Strain–Birefringence Curves for Epoxy Material Batch A at Various Thermal Cycles

3.1.2.3 Polycarbonate Material (Batch B)

Effective stress-strain and birefringence curves were generated for the polycarbonate material (batch B) for thermal cycles consisting of maximum temperatures of 270, 280, and 290° F. The heating-and-cooling rates of these cycles were approximately 5° F per hour and soak times were eight hours. . The effective stress-strain curves are represented in Fig. 15, curves A and C, and Fig. 16. These curves have been nondimensionalized in Fig. 17. The associated strain birefringence curves are shown in Fig. 18, curves A and C, except for T_{max} = 190° F. In this case it was not possible to measure birefringence due to the very high fringe order involved. On the basis of other data, fringe orders exceeding 150 were present in the 0.125-in. thick specimen for the lowest stress level (260 psi).

3.1.2.4 Polycarbonate Material (Batch A)

Two maximum temperatures (260 and 270° F) were used to generate the effective stress-strain curves for batch A. The same heating-and-cooling rates and soak times were used as for batch B. The effective stress-strain curves are shown in Fig. 15, curves B and D. The stress-strain curves have been nondimensionalized and compared with 2024(24ST) aluminum alloy in Fig. 19. The strain-birefringence data are shown in Fig. 18, curves B and D.

3.2 PHOTOELASTO-PLASTIC ANALYSIS OF INFINITE PLATES

3.2.1 Test Procedure

Based upon the results of the calibration phase, a material and thermal cycle was selected which would exhibit an effective stress-strain curve similar to an aluminum alloy. The material selected for use in the infinite plate study was an epoxy resin cured with 10 pbw* of diethanolamine curing agent, batch B. The infinite plate models

---

*Parts by weight

23
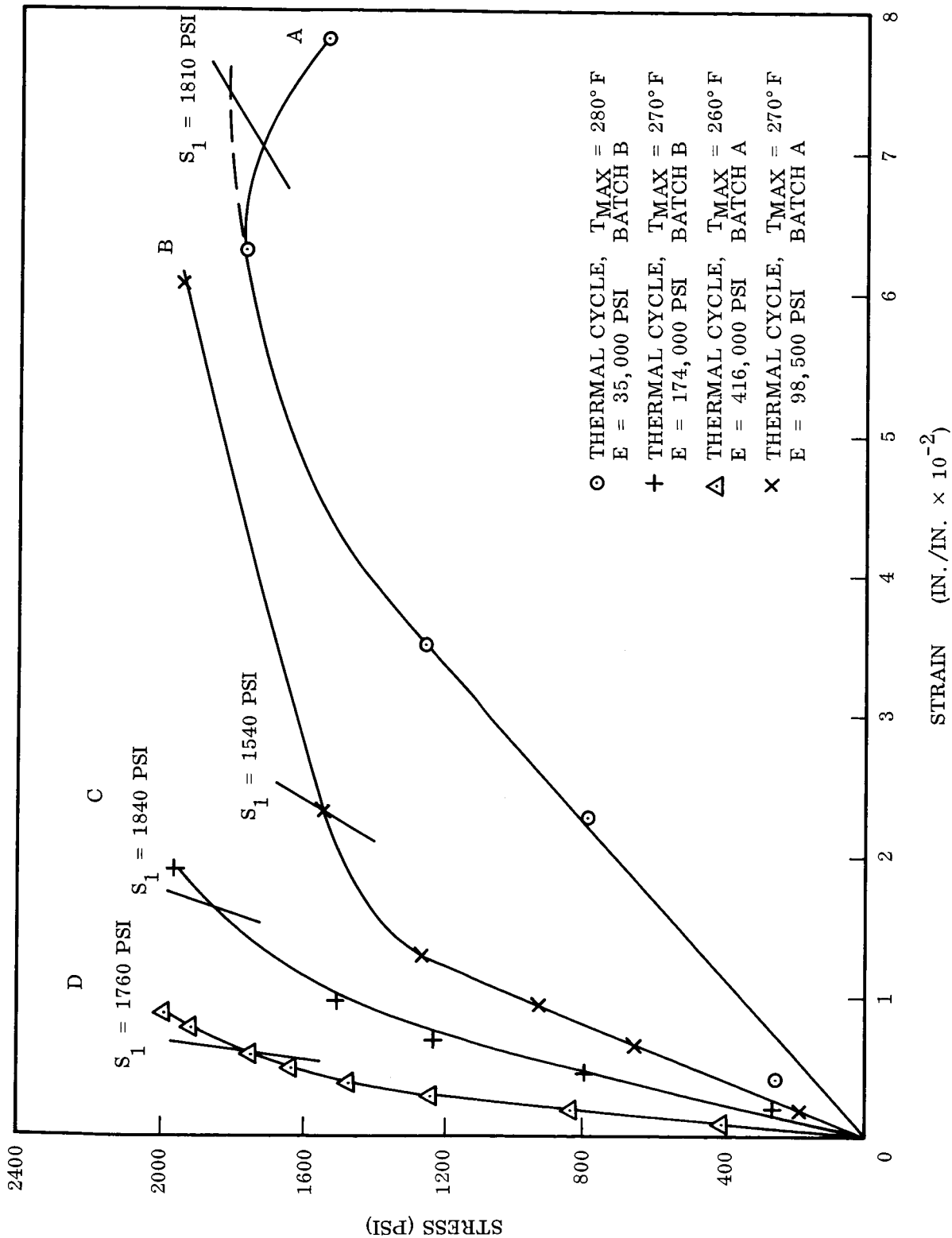
Fig. 15 Effective Stress-Strain Curves for Polycarbonate

24

Fig. 16 Effective Stress-Strain Curve for Polycarbonate

THERMAL CYCLE, $T_{MAX} = 290°F$
E = 8950 PSI

BATCH B

$S_1 = 700$ PSI

STRAIN (IN./IN. $\times 10^{-2}$)

STRESS (PSI)
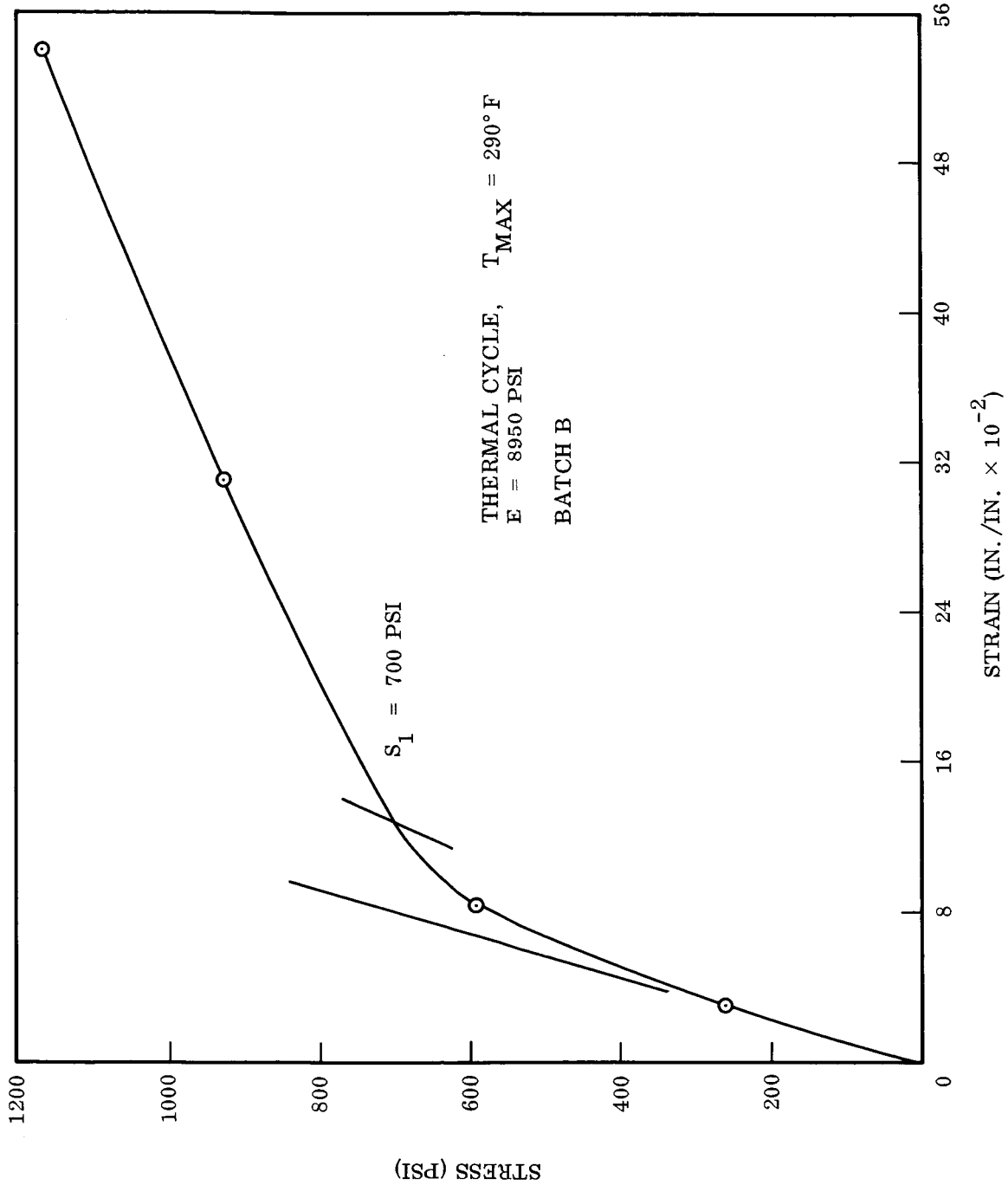
Fig. 17 Non-Dimensionalized Stress-Strain Curve for Polycarbonate Batch B at Various Thermal Cycles

Fig. 18 Strain-Birefringence Curves for Polycarbonate Batch A and B at Various Thermal Cycles

Fig. 19 Non-Dimensionalized Stress-Strain Curves for Polycarbonate Batch A at Various Thermal Cycles

were subjected to a thermal cycle consisting of a maximum temperature of 160° F, heating and cooling rates of 5° F per hour an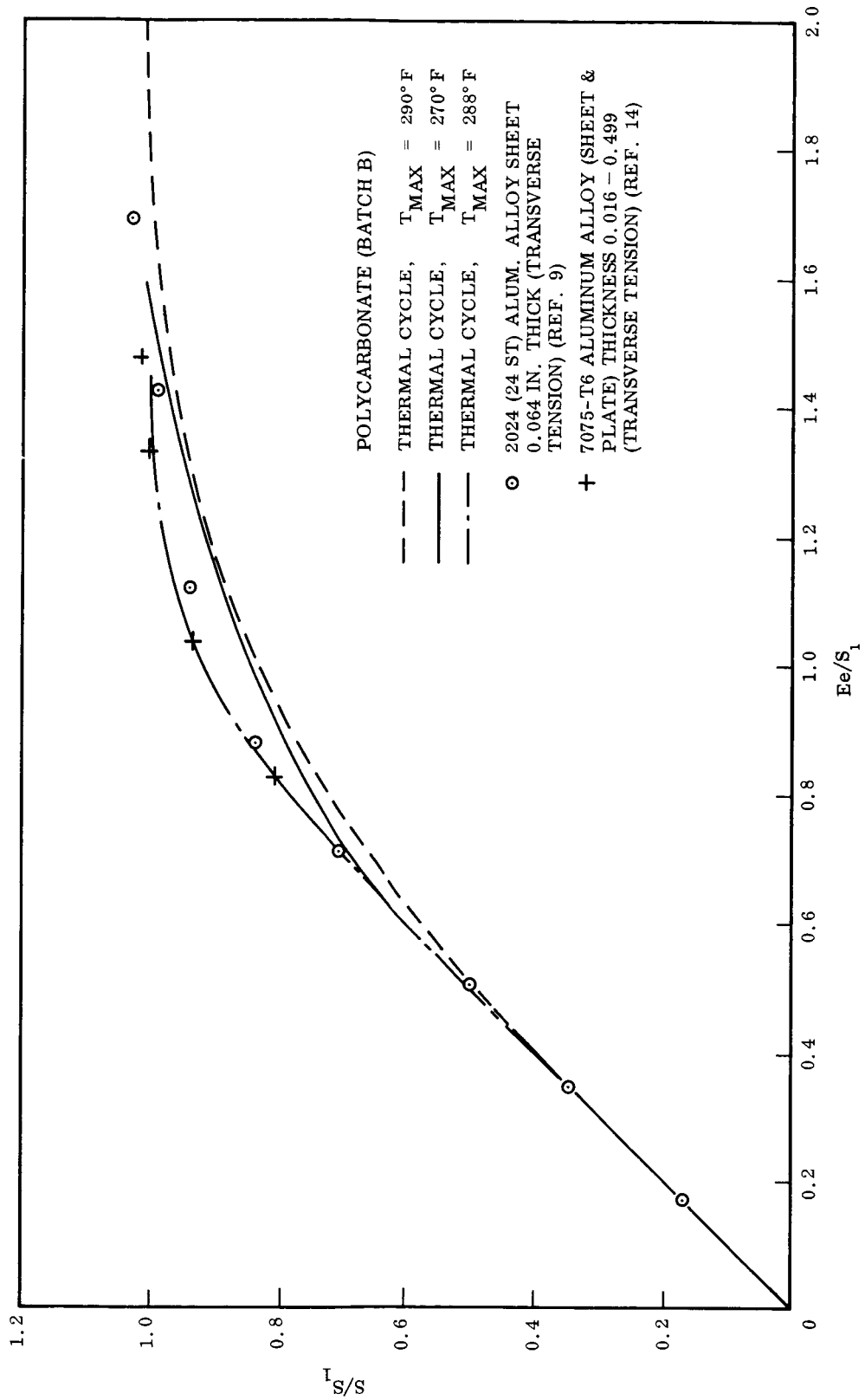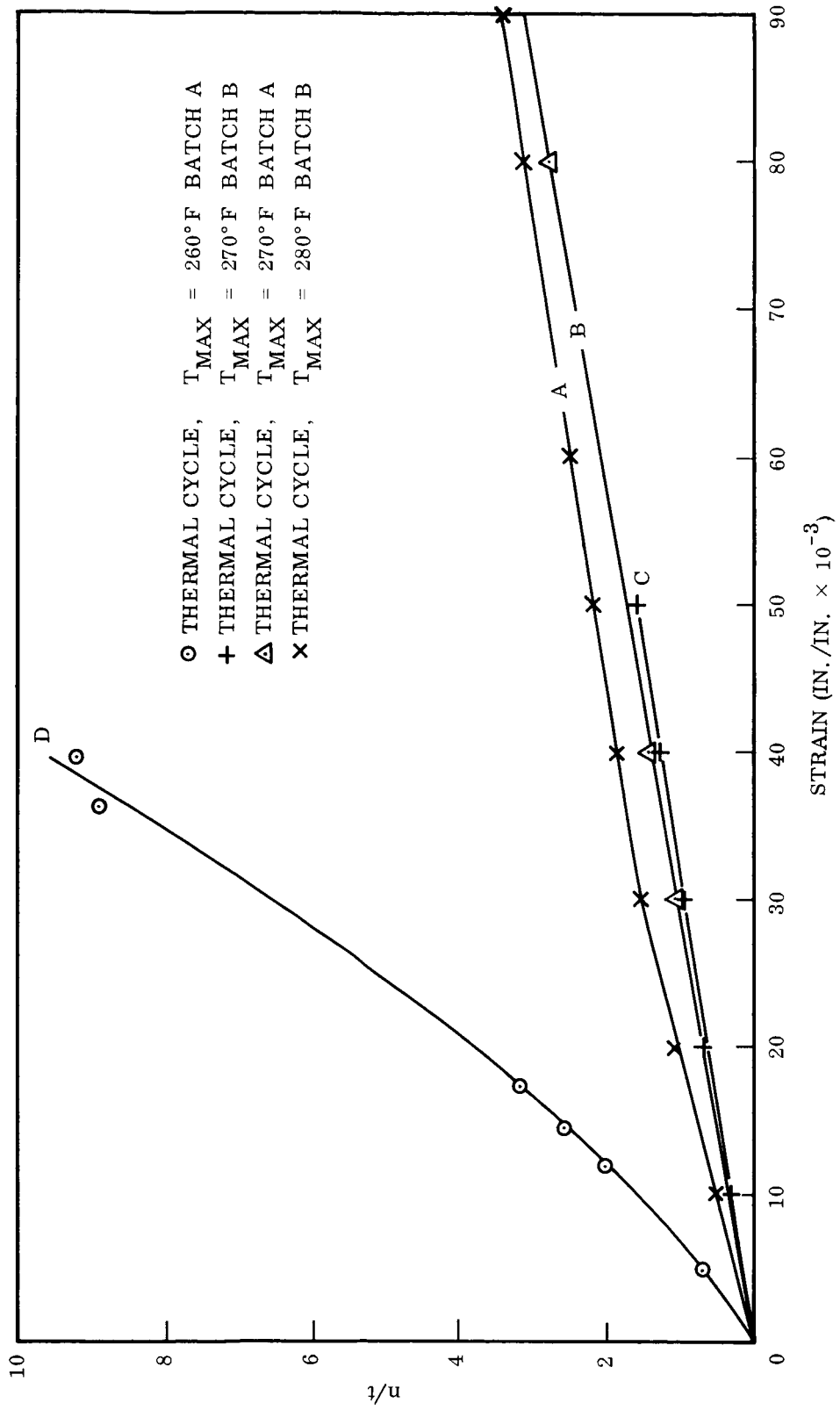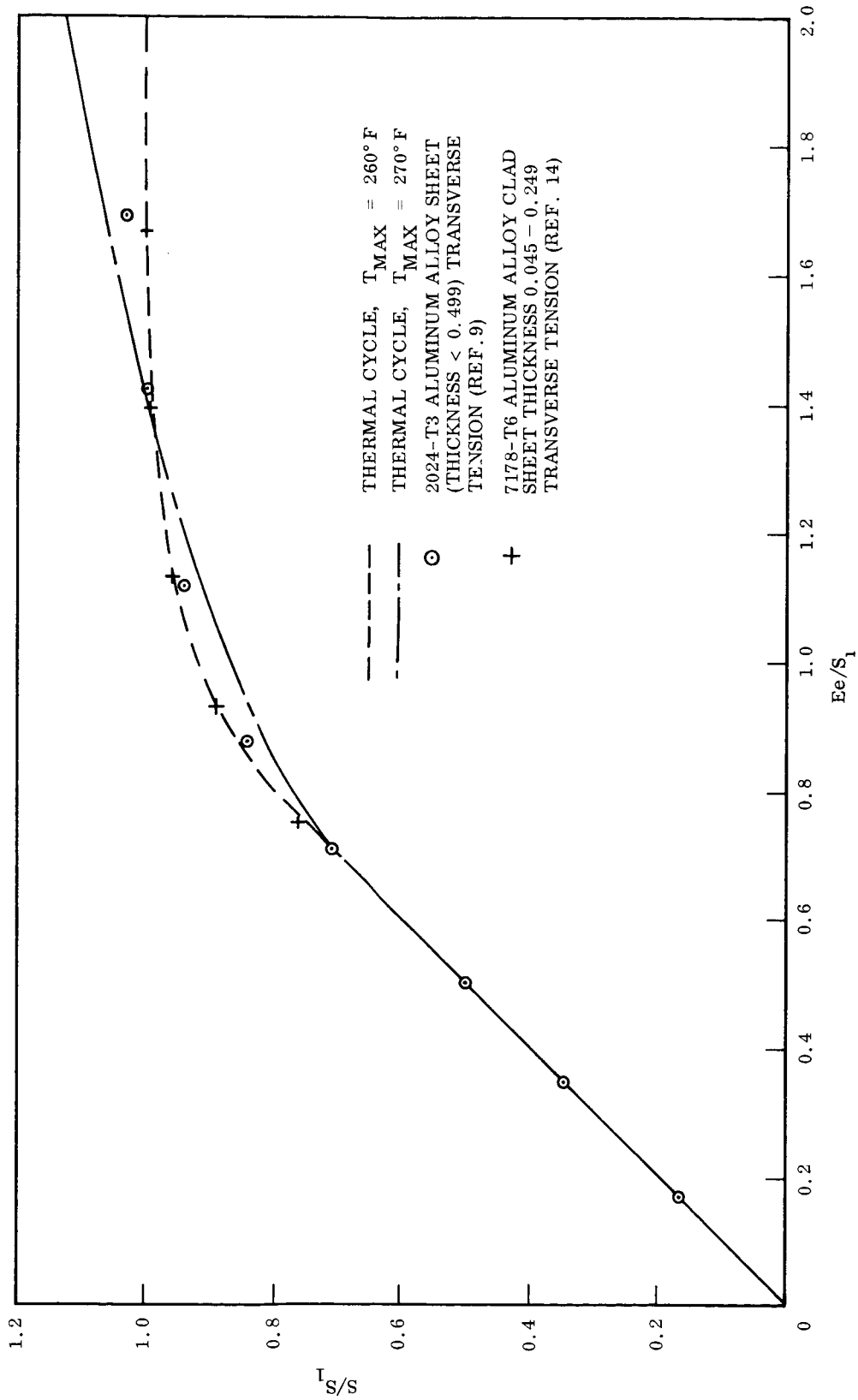d soak time at maximum temperature of two hours while under a constant load. Four infinite plate models of the configuration shown in Fig. 20 were machined from the selected material and batch number. These plates were 4 in. wide and contained a 1/8-in. diameter centrally located hole. Two models each were machined to a thickness of 0.125 in. and 0.400 in. Each plate was subjected to constant tensile load throughout the thermal cycle. The load was applied and controlled by means of a hydraulic ram, hydraulic power supply, and servo control system. The furnace, test frame, hydraulic ram, and associated instrumentation are shown in Fig. 21.

In Fig. 22, the birefringence n/t has been replotted in terms of shear stress (τ) from the curves of strain vs. birefringence and stress vs. strain for epoxy material, batch B, and thermal cycle $T_{max} = 160°$ F. Stresses were determined from birefringence measurements utilizing the curve in Fig. 22.

3.2.2 Experimental Results (Verification Phase)

3.2.2.1 Thin-Plate Models

The thin-plate models had a thickness-to-hole-diameter ratio of 1.0. It was assumed that the condition of plane stress was approximately satisfied. Therefore, only the stress distributions along the y axis were determined. The two thin-plate models were subjected to tensile loading which would produce two different levels of plasticity, namely

$$\sigma_\infty/\sigma_1 = 0.11 \text{ (elastic)} \quad \text{and} \quad \sigma_\infty/\sigma_1 = 0.71$$

The coordinate axes are identified for the thin-plate models in Fig. 23. The thin-plate models were optically viewed with polarized light incident normal to the x-y plane. Observation in this direction provides information concerning the principal
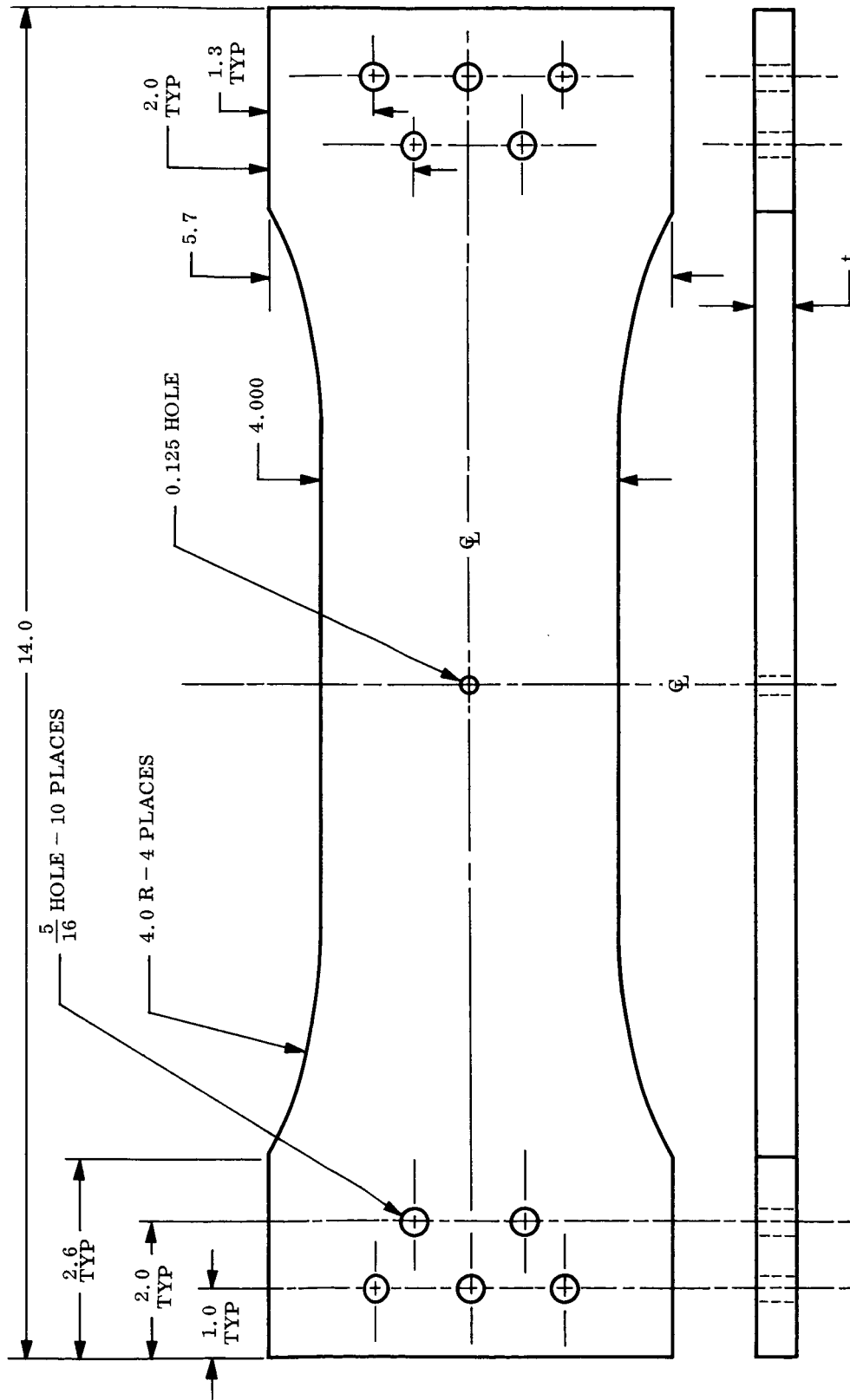
Fig. 20 Infinite Plate Model Configuration

Fig. 21 Hydraulic Ram, Servo Control, Test Frame, Furnace, and Associated Instrumentation for Infinite Plate Study
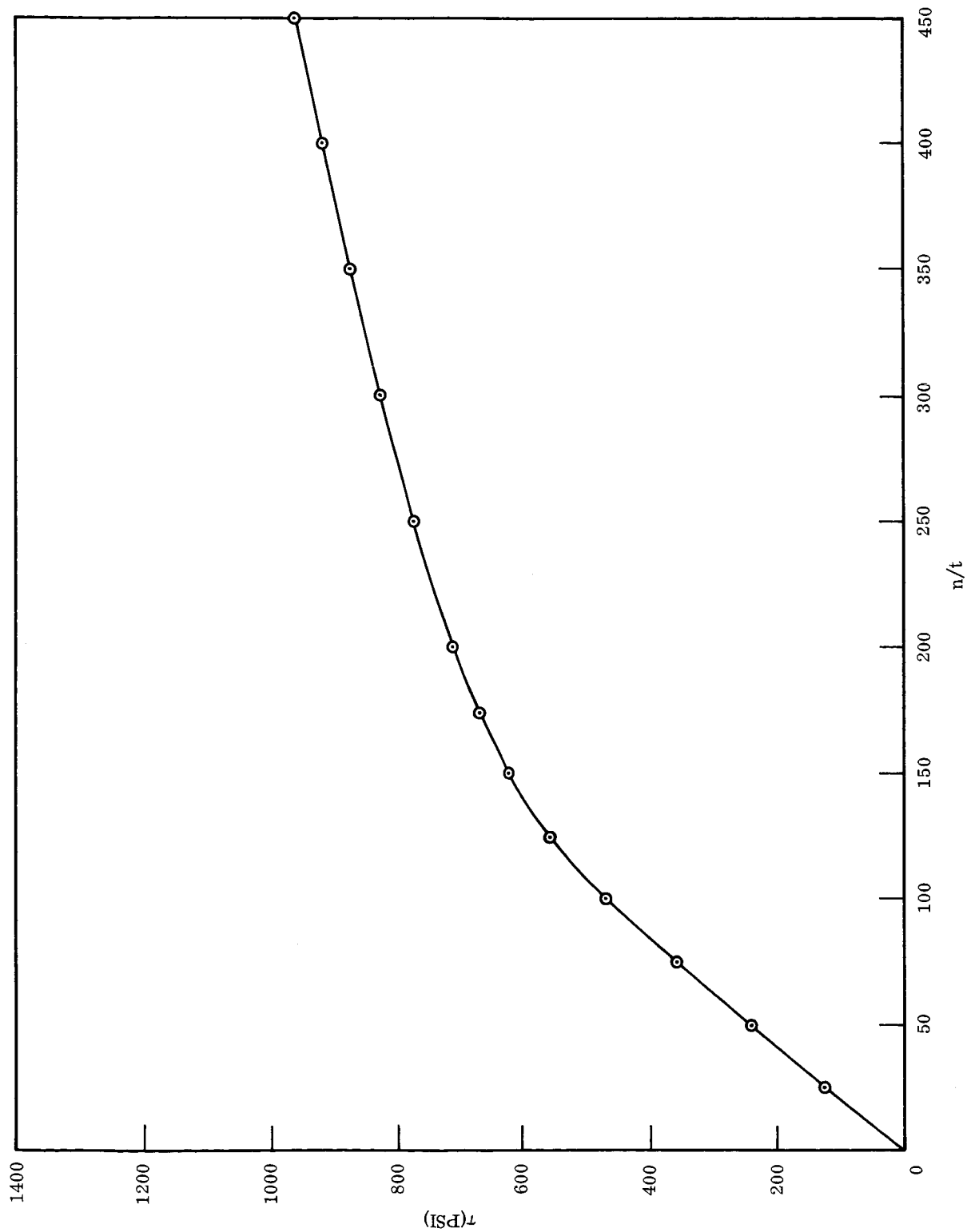
31

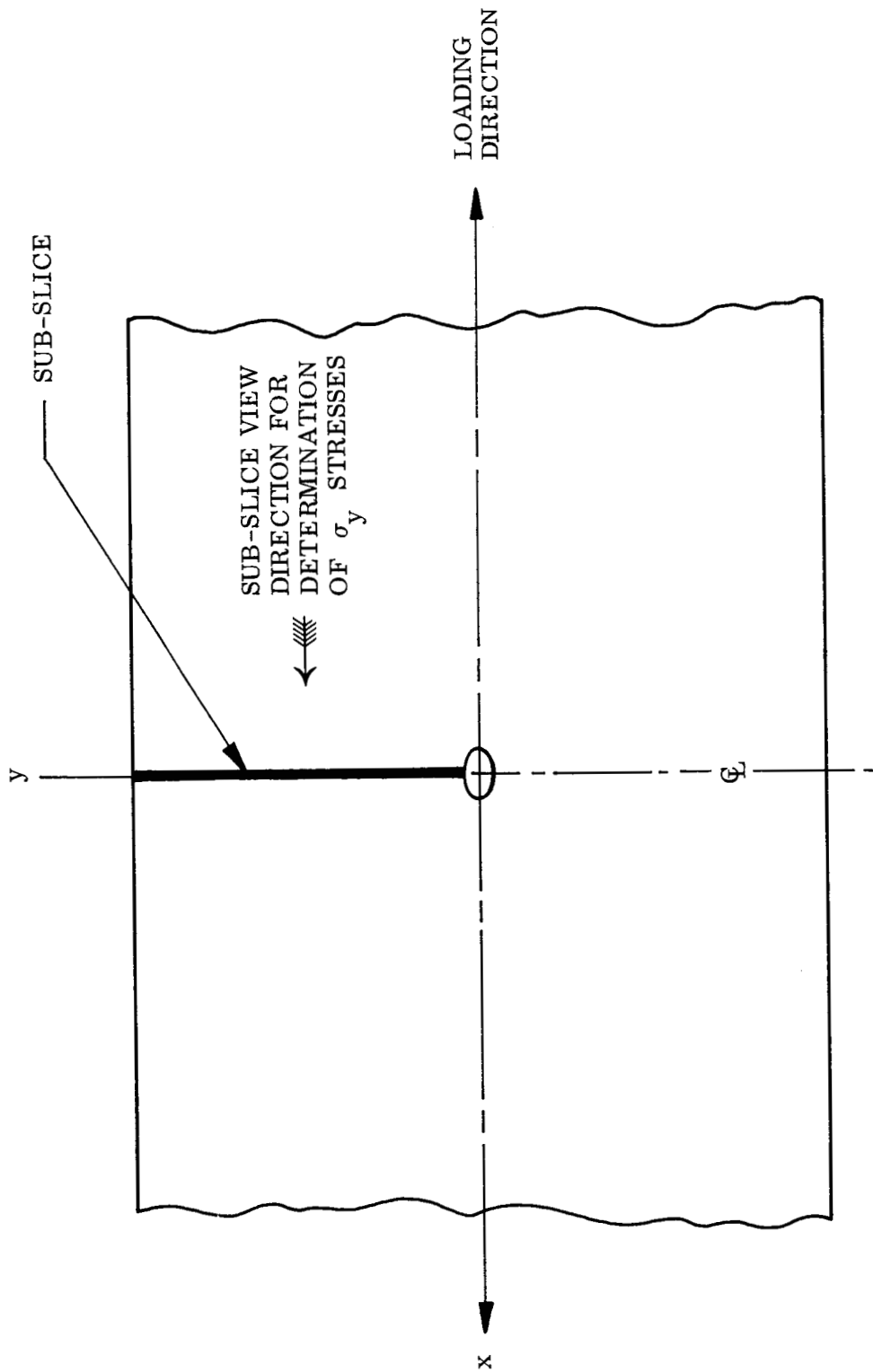Fig. 22 Stress–Birefringence Curve at Thermal Cycle $T_{max} = 160°$ F

32

Fig. 23 Co-ordinate Orientation, Slice Location, and Viewing Direction for Plane Stress Models

LOCKHEED MISSILES & SPACE COMPANY

stress difference in the x-y plane. Fringe order measurements were made along the y axis in the vicinity of the hole using the Tardy compensation technique. It was necessary to reduce the thickness to approximately 0.027 in order to determine a reference fringe. Fringe order measurements along the y axis provide the distribution of the $(\sigma_x - \sigma_y)$ stresses. At the free boundary, $(\sigma_x)_{max}$ could be measured directly. A sub-slice was cut from the specimen, as shown in Fig. 23. Fringe order measurements taken for this sub-slice, when viewed in the x direction, provided the distribution of the σ_y stresses along the y axis. From the distribution of the $(\sigma_x - \sigma_y)$ stresses and the σ_y stresses, the σ_x stress distributions were determined for the two thin plates. The stress distributions for the thin-plate models are shown in Figs. 24 and 25. The stress distributions are plotted in terms of the ratio of the stress at the point σ to the stress in the net section σ_∞ which was determined from P/A.

The infinite plate of $2r_o/h = 1.00$ and load condition of $\sigma_\infty/\sigma_1 = 0.11$ represents an elastic stress distribution. Referring to the effective stress-strain curve shown in Fig. 22, the maximum stress is approximately 160 psi. This is well below the elastic limit.

The dashed curves in Fig. 24 represent the theoretical stress distributions assuming a plane stress condition. The maximum stress concentration factor α_k measured experimentally is 3.3 which is approximately 10 percent higher than the theoretical value for the plane stress condition. The experimental stress distribution represented in Fig. 24 is actually representative of the midplane stresses. Therefore, the high stress-concentration factor tends to indicate the condition of plane stress is violated for a plate with a $2r_o/h$ ratio of 1.00.

According to an analysis of infinite plates with centrally located holes by J. B. Alblas (Ref. 10), a stress concentration factor of 3.1 is indicated for the condition of $2r_o/h = 1.0$ at the midplane.
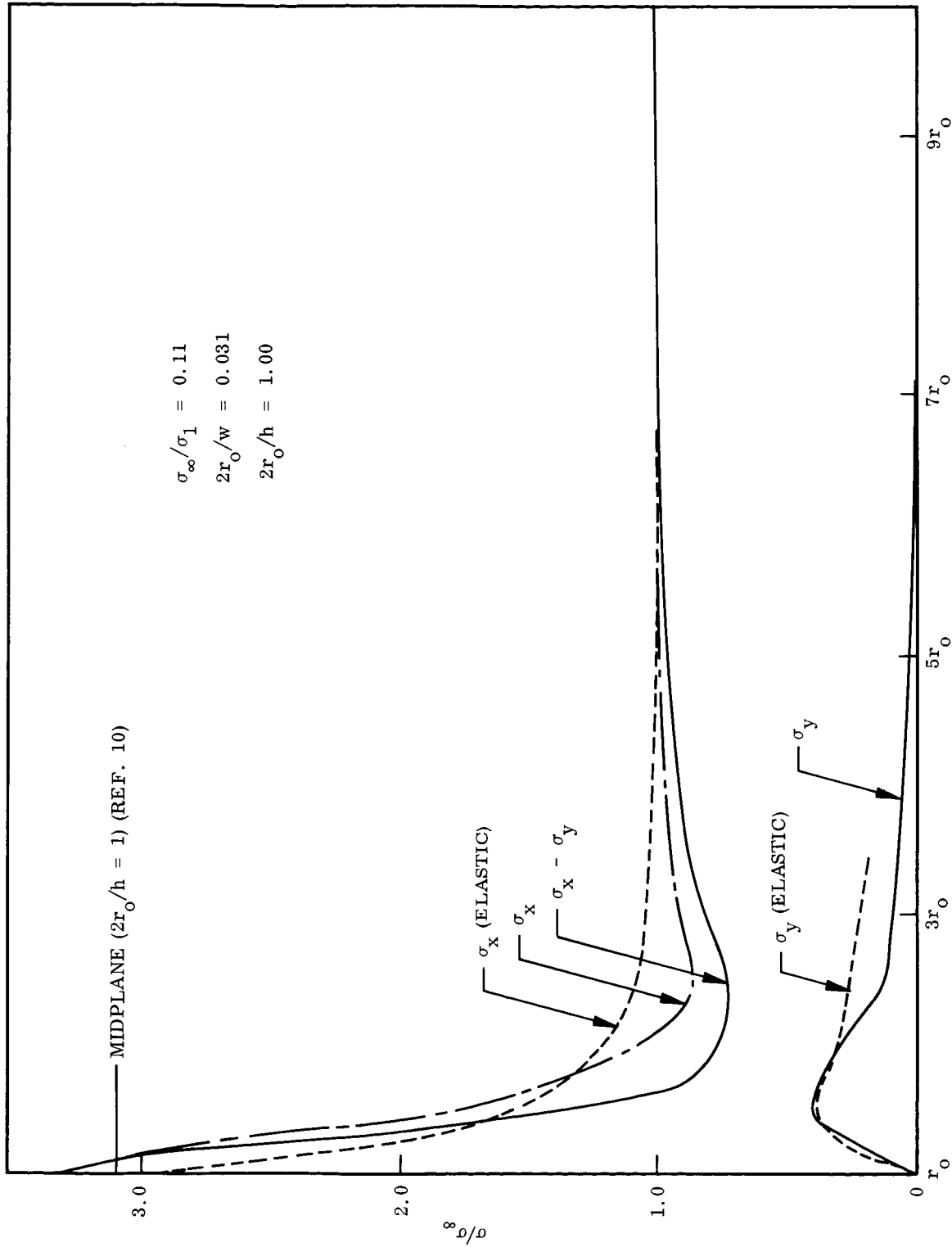
Fig. 24 Elastic-Stress Distribution for Thin Infinite Plate With Centrally Located Hole σ_∞/σ_1

$\sigma_\infty/\sigma_1 = 0.11$

$2r_o/w = 0.031$

$2r_o/h = 1.00$

MIDPLANE ($2r_o/h = 1$) (REF. 10)

σ_x (ELASTIC)

σ_x

$\sigma_x - \sigma_y$

σ_y (ELASTIC)

σ_y

σ/σ_∞

Fig. 25 Elasto-Plastic Stress Distribution for Thin Infinite Plate With Centrally Located Hole $\sigma_\infty/\sigma_1 = 0.71$

ELASTIC (ANALYTICAL)

$\sigma_\infty/\sigma_1 = 0.71$

$2r_o/w = 0.031$

$2r_o/h = 1.0$

σ_x (ELASTIC)

σ_x

PROPORTIONAL LIMIT

σ_y (ELASTIC)

σ_y

σ/σ_∞

For the infinite plate $(2r_o/h = 1.0)$ and load condition $\sigma/\sigma_\infty = 0.71$, considerable plastic flow occurs. The stress disturibution for the midplane of this model is shown in Fig. 25. Here again the dashed curves represent the analytical solution for the plane stress elastic condition.

3.2.2.2 Thick-Plate Models

The thick-plate models had a hole-diameter-to-thickness ratio of 0.33. The two thick-plate models were subjected to tensile loading which would produce two different levels of plasticity, $\sigma_\infty/\sigma_1 = 0.41$ and 0.53.

The slicing scheme used for the thick-plate models is shown in Fig. 26. The diagram in (a) shows the location and orientation of the surface slice and midplane. Observation of these slices in the z direction provided information concerning the distribution of $(\sigma_x - \sigma_y)$ stresses as a function of y at z = 0 and z = h/2.

Assuming symmetry of stresses at opposite sides of the hole, a slice was prepared for determination of the σ_z stresses. The slice location and orientation for determination of σ_z stresses is shown in (b) of Fig. 26. The slice was observed in the x direction. Optical measurements, performed on this slice for z = h/2 as a function y, provided for the distribution of the σ_y stresses as a function y. The σ_x stress does not produce an optical effect for the slice because observation is in the x direction.

Optical measurements, for the slice in (b) of Fig. 26, taken for z = 0 along the y axis, provide the distribution of the σ_z stresses as a function of y at z = 0 where the σ_z stresses are maximum, assuming σ_y constant through the thickness.

The stress distribution for the thick infinite plate $(2r_o/h = 0.31)$, loaded to $\sigma_\infty/\sigma_1 = 0.41$, is shown in Fig. 27. The dashed curves represent the analytically determined stress distribution for the elastic plane stress condition. Also shown is the distribution of the σ_z stresses at the midplane where they are a maximum.
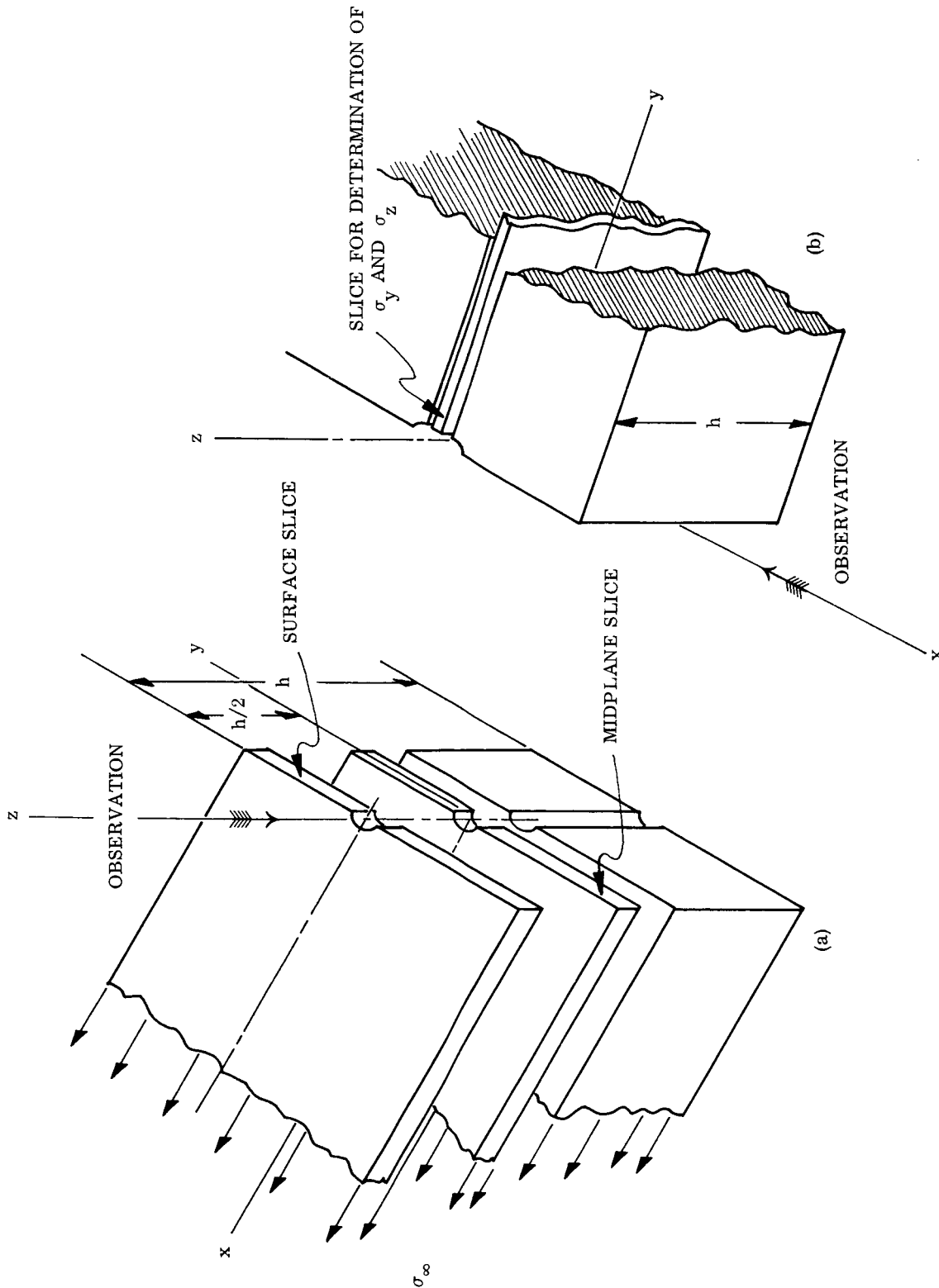
Fig. 26 Co-ordinate Orientation, Slice Location, and Viewing Direction for Elasto-Plastic Models

SLICE FOR DETERMINATION OF σ_y AND σ_z

(b)

OBSERVATION

z

y

x

h

SURFACE SLICE

MIDPLANE SLICE

OBSERVATION
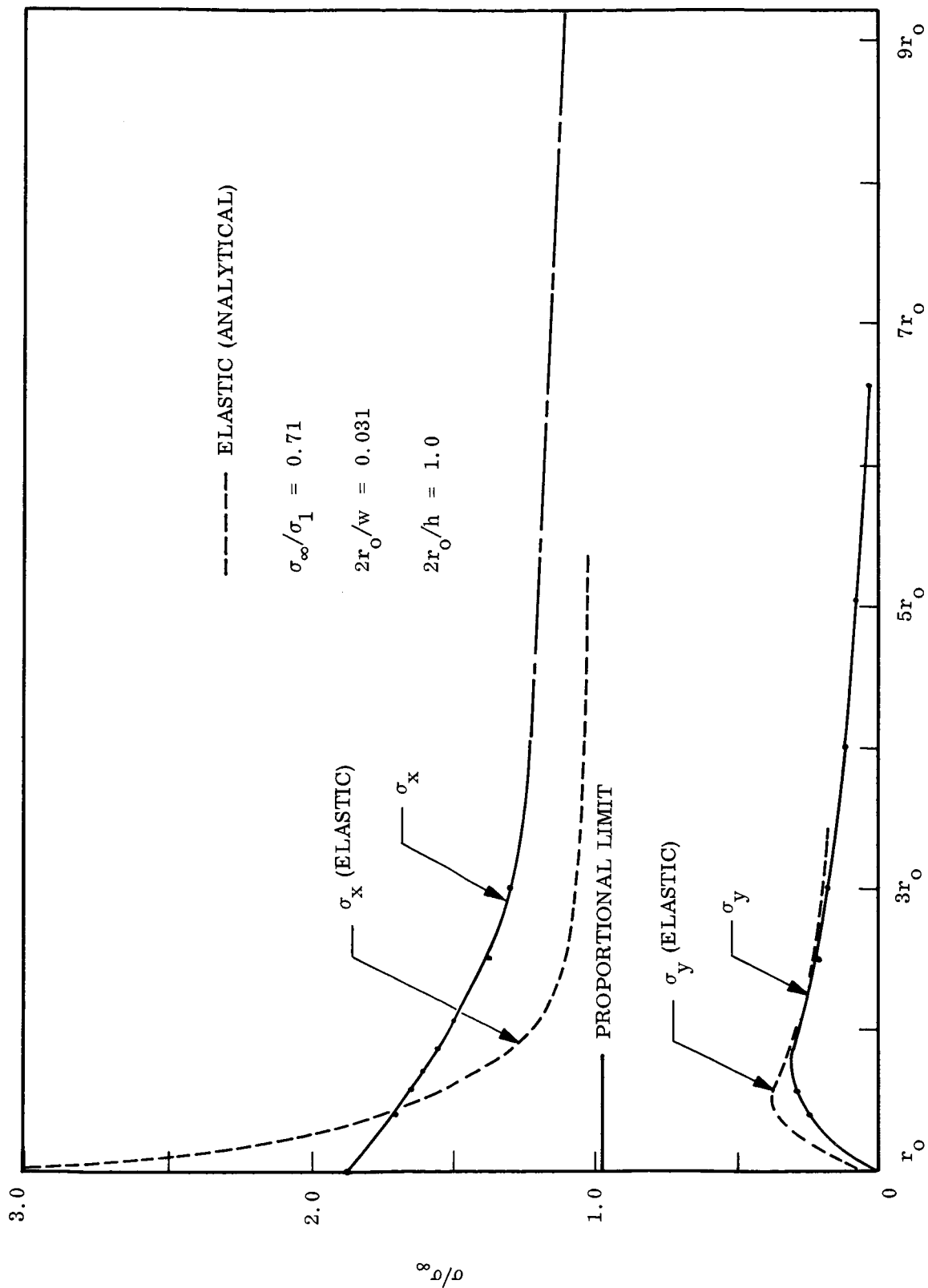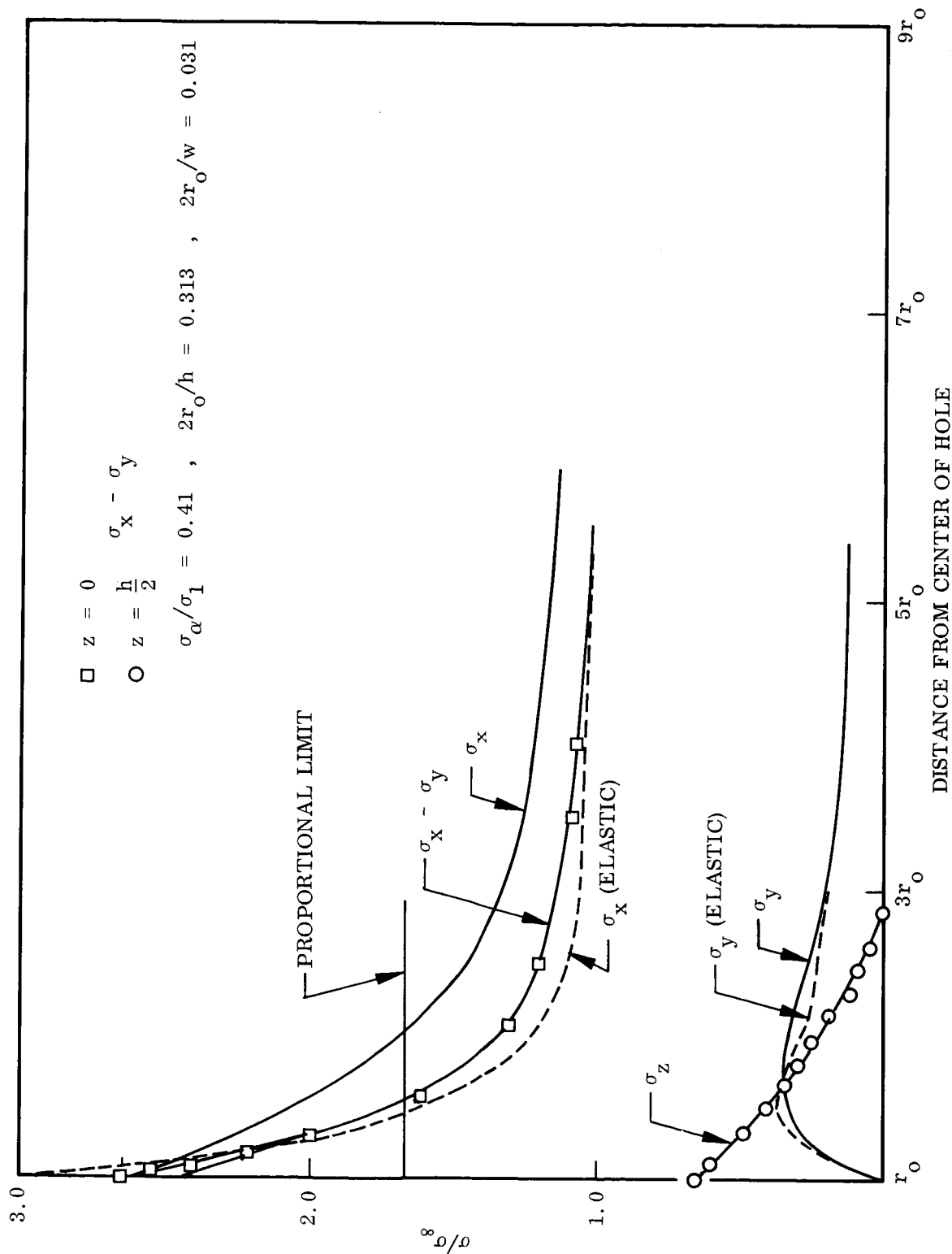
z

y

x

h

h/2

σ^8

(a)

38

Fig. 27 Elasto-Plastic Stress Distribution for Thick Infinite Plate
With Centrally Located Hole $\sigma_\infty / \sigma_1 = 0.41$

The stress distribution for the thick infinite plate ($2r_o/h = 0.31$) loaded to $\sigma_\infty/\sigma_1 = 0.53$ is shown in Fig. 28. Here, again, the dashed curves represent the analytically determined elastic plane stress condition. Figure 29 shows a typical frozen fringe order pattern for slices removed from the thick plate models used for determination of $\sigma_x - \sigma_y$ stresses.

3.3 DISCUSSION OF RESULTS

3.3.1 Calibration Phase

The effective stress-strain curves generated during the course of this program were nondimensionalized by plotting stress S/S_1 versus strain E_e/S_1, where S_1 represents the secant yield strength for $0.7E$. These curves were compared with nondimensionalized stress-strain curves for several aluminum alloys plotted in terms of the same parameters. If similarity exists between the effective stress-strain curve for the photoelasto-plastic material and an aluminum alloy, they will yield the same nondimensional stress-strain curves.

It was found that the epoxy material (batch B) yields an effective stress-strain curve similar to 2024-T3 aluminum alloy (transverse tension) when subjected to a thermal cycle consisting of a heating-and-cooling rate of 5° F per hr and any maximum temperature from 144° F through 160° F. The epoxy material (batch A) yielded an effective stress-strain curve which simulates the uniaxial stress-strain behavior of 7178-T6 aluminum alloy alclad sheet in transverse tension for a thermal cycle of heating-and-cooling rate of 5° F per hr and a maximum temperature of 165° F.

The similarities mentioned above consider cases where the nondimensionalized stress-strain curves are almost identical. However, the epoxy resin could be used to approximate almost any of the aluminum alloys for which the stress-strain curve has a gradual change in slope in the nonlinear range to determine empirical data concerning the elasto-plastic stress distributions resulting from flow.

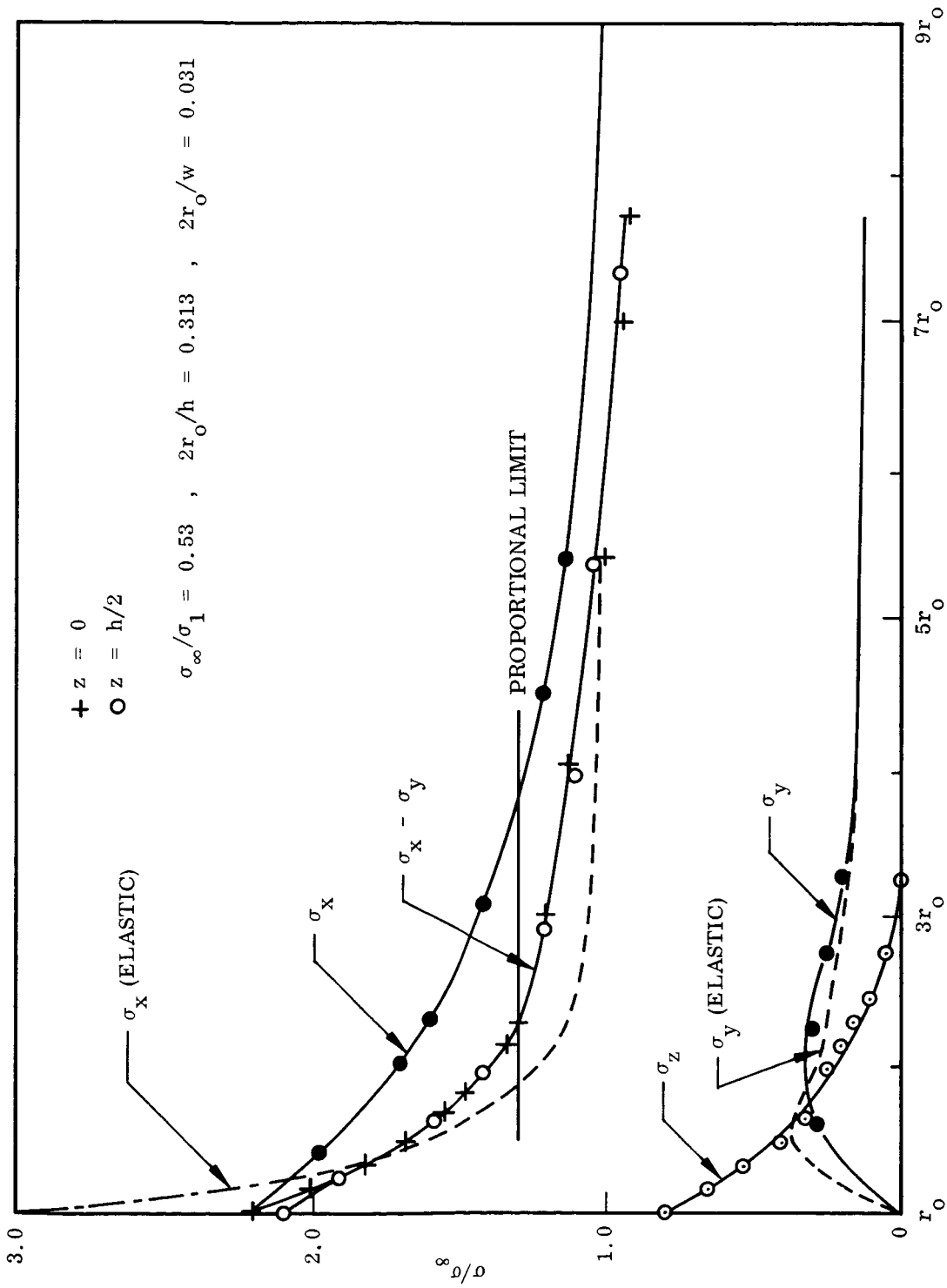Fig. 28 Elasto-Plastic Stress Distribution for Thick Infinite Plate
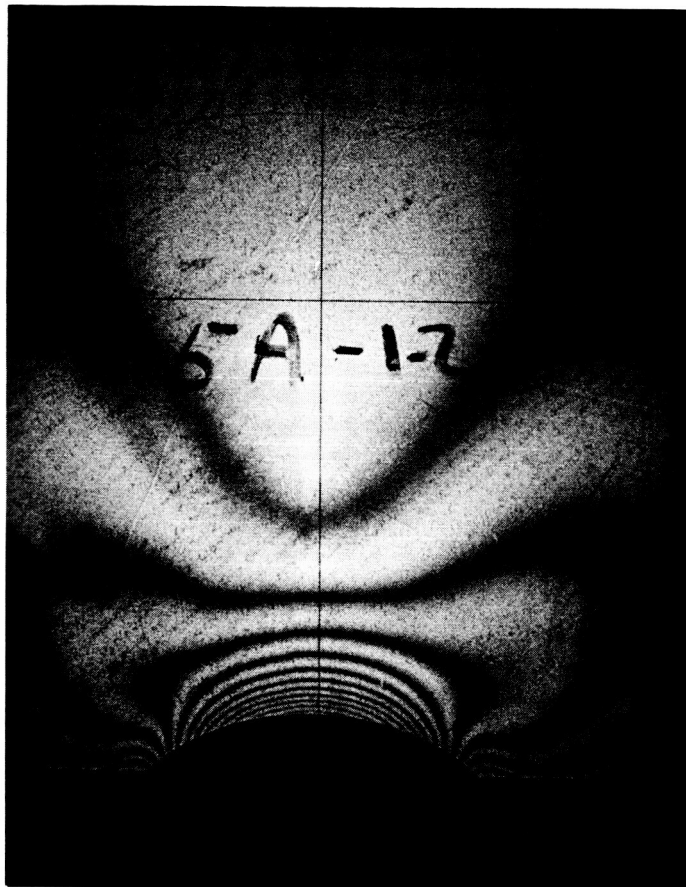With Centrally Located Hole $\sigma_\infty/\sigma_1 = 0.53$

41

Fig. 29 Typical Photoelasto-Plastic Fringe Pattern for
Midplane Slice in Thick Infinite Plate in Vicinity
of Hole

Also, the epoxy material possesses very good machinability, making it possible to prepare the very thin slices (to 0.005 in.) required for three-dimensional analysis in the vicinity of sharp notches.

The polycarbonate material can be used to approximately simulate most aluminum alloys which exhibit gradual change in slope for their stress-strain curve in the non-linear range. However, the high residual stress in the as-received condition and the very poor machinability would make it virtually impossible to study three-dimensional problems where slicing is required.

3.3.2 Infinite Plate Study (Verification Phase)

Utilizing an effective stress-strain and associated birefringence curve generated during the calibration phase, an analysis of the elasto-plastic stress distributions in infinite plates with centrally located holes was conducted.

The stress concentration factors are shown in Fig. 30 as a function of the level of plasticity (σ_∞/σ_1). The thin infinite plate $(2r_0/h)$ was loaded to $\sigma_\infty/\sigma_1 = 0.11$. This represented an elastic condition. The specimen was milled to 0.027-in. thick to determine a reference fringe for application of the Lardy method of compensation assuming a plane-stress condition, therefore representing a midplane slice. The measured stress-concentration factor was about 10 percent higher than for the theoretical plane-stress value. This would indicate that the assumption of plane stress for this condition was not correct. J. B. Alblas (Ref. 10) has computed an elastic stress concentration of 3.1 at the midplane of this condition $(2r_0/h)$. The experimental value is about 6-1/2 percent higher than computed by Alblas. The thin plate loaded to $\sigma_\infty/\sigma_1 = 0.7$ yields an experimental stress concentration factor of 1.88. This value is approximately 4-1/2 percent higher than predicted by Budiansky (Ref. 11), and 14 percent higher than Neuber's theory predicts. The value predicted by Budiansky is for stress-strain curve with shape factor n = 9, whereas n = 7 for the experimental case. Neuber's theory (Ref. 12) considers any arbitrary stress-strain curve; the curve in Fig. 30 was derived from Neuber's theory for the stress-strain curve of the model material.

3.3

ELASTIC MIDPLANE (REF. 10)
$2r_0/h = 1$

3.0

2.5

σ/σ_∞

n=9 (REF. 11)

2.0

1.5

(REF. 12)

1.0

⊙ MIDPLANE STRESS CONCENTRATION

+ SURFACE STRESS CONCENTRATION

△ CALCULATED FROM:

0.5

$\sigma/\sigma_\infty = 1 + 2 (E_\sigma/E_\infty)$

(REF. 13)

0   0.2   0.4   0.6   0.8   1.0
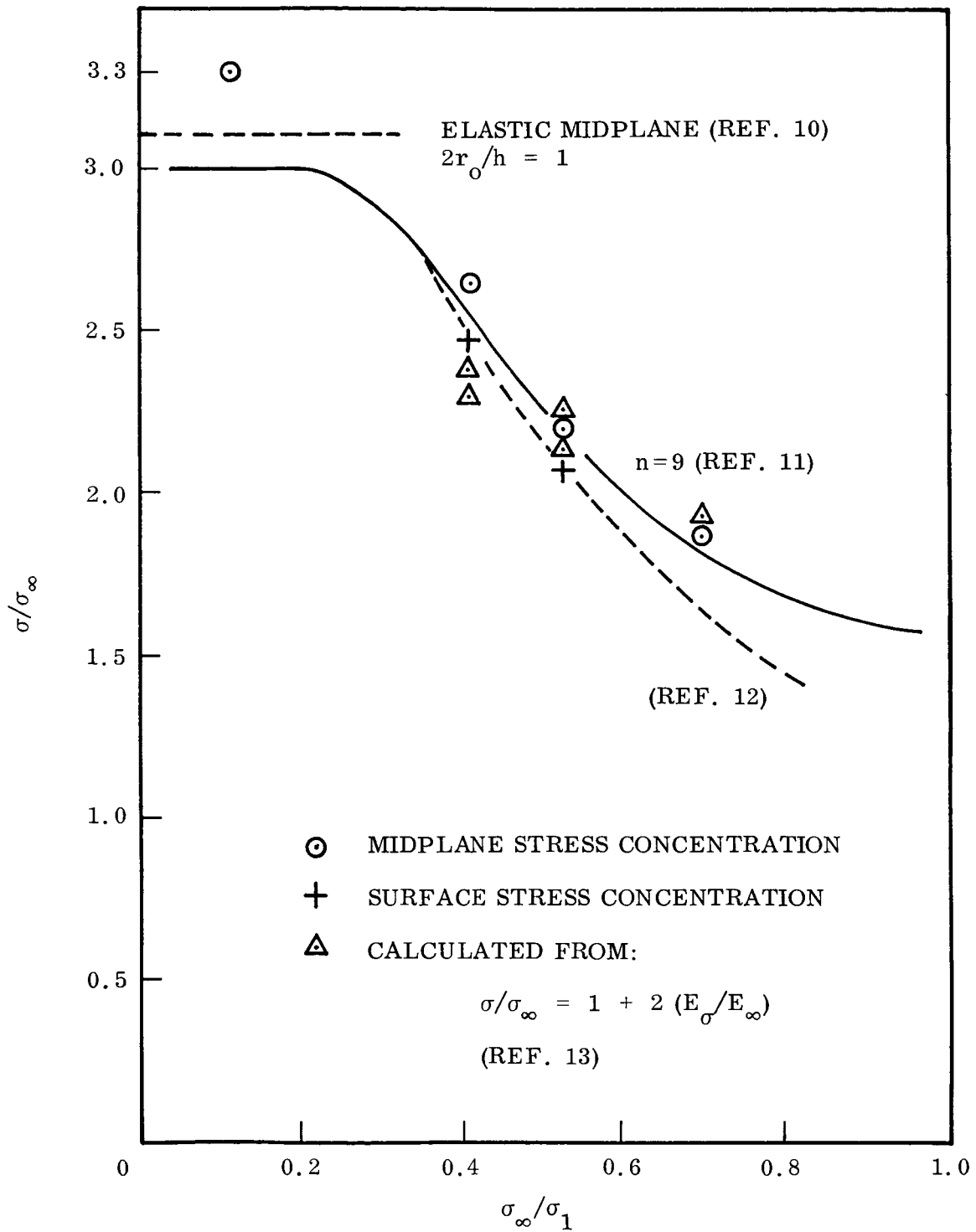
σ_∞/σ_1

Fig. 30 Stress Concentration Factors for Various Levels of Plasticity

44

The thick-plate models were tested at $\sigma_\infty/\sigma_1 = 0.41$ and 0.53 . The stress distributions were determined for a surface slice and for a midplane slice. The measured stresses were higher at the midplane than at the surface in the vicinity of the hole. At a short distance from the hole the stresses did not vary through the thickness. The surface and midplane stress concentrations are shown in Fig. 30. The stress concentration factors at the midplane agree very well with Budiansky (Ref. 11), and the surface stress concentration factors agree with Neuber. Due to the higher σ_x stresses at the midplane of the thick-plate models, there arises a tensile σ_z which is a maximum at midplane and edge of the hole. The σ_z stresses are zero at the surface of the thick specimens. For $\sigma_\infty/\sigma_1 = 0.41$ the maximum $\sigma_z/\sigma_\infty = 0.65$ and for $\sigma_\infty/\sigma_1 = 0.53$ the maximum $\sigma_z/\sigma_\infty = 0.8$.

3.4 CONCLUSIONS

Based upon the experimental work of the program concerning the development of a photoelasto-plastic method to study the stresses associated with plastic flow in the vicinity of a notch, the following conclusions have been reached:

(1) It is possible to generate an effective stress-strain curve by the "frozen" stress technique using an appropriate thermal cycle whose maximum temperature is significantly below the critical temperature of the model material.

(2) The above-mentioned method can be used to determine the stress concentration factors for elasto-plastic situations.

(3) The method also yields realistic information concerning stress variation through plate thickness caused by plastic flow. No theory exists for an accurate comparison.

Section 4

REFERENCES

1. H. Neuber, "Theory of Notch Stresses," AEC-TR 4547, 1961

2. M. W. Brossman, and T. A. Kies, "Energy Release Rates During Fracturing of Perforated Plates," U.S. Naval Research Laboratory, Memorandum Report No. 370, April 1955

3. A. Wells, and D. Post, "The Dynamic Stress Surrounding a Running Crack — A Photoelastic Analysis," Proceedings of the Society for Experimental Stress Analysis, XVI, No. 1, 1957, pp. 69−92

4. J. Dixon, "Stress Distribution Around a Central Crack in a Plate Loaded in Tension; Effect of Finite Width of Plate," Journal Roy. Aeron. Soc., Vol. 64, 1960, pp. 141−145

5. J. Dixon, "Some Studies of Elastic-Plastic Strain Distributions in Flat Bars Containing Holes and Notches," DSIR Report No. PM 303, National Engineering Laboratory, East Kilbride, Glasgow, 1961

6. K. Kawata, "Analysis of Elasto-Plastic Behavior of Metals by Means of Photoelastic Coating Method," Jour. Sci. Res. Inst., Vol. 52, Tokyo, 1958, pp. 17−40

7. W. Gerberich, "Stress Distribution About a Slowly Growing Crack Determined by Photoelastic Coating Method," Experimental Mechanics, Dec 1962, p. 359

8. M. Frocht, and M. Leven, "On the State of Stress in Thick Bars," J. App. Phys., 13 May 1942

9. W. Ramberg, and W. Osgood, "Description of Stress-Strain Curves by Three Parameters," NACA TN 902, July 1943

10. J. B. Alblas, "Theorie von de driedimensionale spanningstoestand in een doorboorde ploat," Amsterdam, 1957

11. B. Budiansky, and R. Vidensek, "Analysis of Stresses in the Plastic Range Around a Circular Hole in a Plate Subjected to Uniaxial Tension," NACA TN 3542

12. H. Neuber, "Theory of Stress Concentration for Shear-Strained Prismatical Bodies with Arbitrary Nonlinear Stress-Strain Law," J. Appl. Mechanics, Dec 1961, p. 544

13. H. Hardrath and L. Ohman, "A Study of Elastic and Plastic Stress Concentration Factors Due to Notches and Fillets in Flat Plates," NACA Report 1117

14. ANC-5 Handbook